AIMS Mathematics, 11(3): 8716–8761.
DOI: 10.3934/math.2026359
Received: 29 December 2025
Revised: 02 March 2026
Accepted: 05 March 2026
Published: 31 March 2026

https://www.aimspress.com/journal/Math

Research article

A fractal-fractional chemo-immune model for non-muscle-invasive bladder cancer: Analysis and simulation

Sagar R. Khirsariya[1,*] **and Saud Fahad Aldosary**[2]

[1] Department of Mathematics, Marwadi University, Rajkot, Gujarat-360003, India

[2] Department of Mathematics, College of Science and Humanities in Alkharj, Prince Sattam bin Abdulaziz University, Alkharj 11942, Saudi Arabia

* **Correspondence:** Email: ksagar108@gmail.com.

Abstract: This research presents a novel mathematical study for analyzing the chemo-immune dynamics of non-muscle-invasive bladder cancer (NMIBC). We generalize a foundational three-compartment model (Mitomycin-C, Tumor, Effector-cells) by employing the fractal-fractional (FF) differential operator in the Caputo sense, characterized by a fractional order α and a fractal dimension β. This advanced operator is uniquely suited to capture the non-local memory effects inherent in immune system activation and the fractal (non-Euclidean) nature of the tumor microenvironment. We first establish the model's mathematical integrity by rigorously proving the existence, uniqueness, positivity, and boundedness of its solutions. The long-term behavior of the system is then analyzed, centered on the derivation of the basic reproduction number ($\mathcal{R}_0$). We demonstrate that the disease-free equilibrium is globally asymptotically stable if $\mathcal{R}_0 \leq 1$, while a unique endemic (tumor) equilibrium emerges and gains stability if $\mathcal{R}_0 > 1$, indicating a transcritical bifurcation. For the numerical solution, we develop a semi-analytical scheme using the fractal-fractional Adomian decomposition method (FF-ADM) and validate its high accuracy against established numerical methods. Extensive numerical simulations are presented, including 2D and 3D plots, which visualize the profound impact of the fractional parameters α and β on the system's trajectory, revealing that they significantly alter the time to tumor clearance. A comprehensive sensitivity analysis identifies the most critical parameters for controlling the disease, and 3D bifurcation plots illustrate the thresholds between tumor elimination and persistence. This work provides a more realistic and flexible tool for understanding NMIBC, with direct implications for optimizing treatment strategies.

Keywords: non-invasive bladder cancer; fractal-fractional derivative; stability analysis; Adomian decomposition method; basic reproduction number
Mathematics Subject Classification: 92C50, 34A08, 34D20, 37N25

1. Introduction

Bladder cancer (BC) represents a significant global health challenge, ranking as one of the most common malignancies worldwide [1]. The majority of newly diagnosed cases, approximately 70-80%, are classified as non-muscle-invasive bladder cancer (NMIBC), which is confined to the mucosa or submucosa [2]. The standard treatment for NMIBC involves transurethral resection of the bladder tumor (TURBT), followed by adjuvant intravesical immunotherapy, such as Bacillus Calmette-Guérin (BCG), or chemotherapy, such as Mitomycin C (MMC) [3, 4]. Despite these interventions, NMIBC has a notoriously high recurrence rate, exceeding 50% within five years, and a significant risk of progression to muscle-invasive disease [5]. This clinical challenge underscores the urgent need for optimized treatment strategies and a deeper understanding of the tumor-immune dynamics under therapy.

Mathematical modeling provides a powerful, quantitative framework for integrating biological mechanisms and clinical data to unravel the complexities of cancer dynamics [6, 7]. In the context of bladder cancer, various models have explored tumor growth, immune response, and treatment efficacy [8, 9]. Recently, Yosef and Bunimovich-Mendrazitsky proposed a novel ordinary differential equation (ODE) model to describe the interplay between the MMC chemotherapy drug, NMIBC tumor cell population, and the responding effector-immune cells [3]. This model, built on biological data, provides critical insights into the conditions for tumor elimination versus recurrence.

However, classical integer-order differential equation models, including the aforementioned one, are formulated based on the Markovian assumption. They operate under the principle that the future state of the system depends solely on its current state, disregarding the system's history. This assumption is a profound limitation in biology, where processes such as cell proliferation, immune activation, and drug response are known to be non-local in time and possess significant "memory" [10, 11]. For example, an effector cell's activation depends on a history of past encounters with tumor antigens, not just the current concentration.

To overcome these limitations, fractional calculus has emerged as a powerful framework [12–14] and has been extensively applied in mathematical biology [15, 16]. Owing to their inherent memory and hereditary characteristics, fractional-order derivatives provide a more realistic representation of complex biological processes [17, 18]. Consequently, a wide range of fractional-order models have been developed in quantum mechanics [19], epidemiology [15,20], and oncology [21,22], consistently demonstrating superior agreement with real-world data when compared to classical integer-order formulations.

Recent studies include advanced fractional modeling of diabetes and comparative analyses of numerical methods such as the Adams–Bashforth–Moulton and Laplace–Adomian–Padé methods [23], numerical analysis of time-fractional cancer models with different types of net killing rate [24], a fractal-fractional-order modeling approach to understanding stem cell-chemotherapy combinations for cancer [25], evaluating the stability and efficacy of fractal-fractional models in reproductive cancer apoptosis with ABT-737 [26], hybrid Euler–Lagrange formulations for glucose–insulin dynamics [27], development of pure multi-order fractional optimal control problems with constraints using QP and LP techniques [28], and an efficient method for a variety of fractional time-delay optimal control problems with fractional performance indices [29]. Additional contributions address diverse applications, including computer virus propagation using ABC fractional derivatives with

Mittag–Leffler kernels [30], tumor-immune interaction dynamics [31], breast cancer modeling with chemotherapy-induced adverse effects [32], and bifurcation analysis of fractional-order Hepatitis B epidemic models [33]. Further numerical and analytical investigations encompass fractional SCIR models for pneumonia [34] and chlamydia dynamics with protected intimacy [35].

More recently, the concept has been extended to fractal-fractional (FF) operators [36, 37]. These operators generalize fractional calculus by introducing a second parameter, the fractal dimension β, in addition to the fractional order α. The fractional order α incorporates the system's memory, capturing the history-dependent nature of immune cell activation (immune memory) and the residual retention of the chemotherapy drug in tissues. Simultaneously, the fractal dimension β characterizes the irregular, self-similar geometry of the tumor vasculature. This structural complexity restricts the movement of agents, leading to anomalous diffusion (sub-diffusion) of both MMC and effector cells, which deviates from the standard Brownian motion assumed in classical models. This dual-parameter implementation is exceptionally potent, as it allows for the simultaneous description of memory effects (via α) and the fractal spatial structure (via β) of the medium in which the dynamics occur [36, 38]. Biological tissues, particularly tumor microenvironments, are well-established as fractal structures, and their geometric complexity inherently affects diffusion and interaction rates [7, 39]. Therefore, a fractal-fractional model is a logical and powerful extension for capturing the heterogeneous and non-local dynamics of tumor-immune interactions [21, 40, 41].

To date, the valuable ODE model for NMIBC chemotherapy proposed in [3] has not been analyzed within a fractal-fractional scheme. This paper aims to fill this gap. We reformulate the NMIBC model using the Caputo-type fractal-fractional derivative, which combines a power-law kernel for memory with a fractal dimension parameter. This new model provides a richer and more flexible structure for exploring the system's dynamics.

This manuscript is structured as follows. In Section 2, we present the formulation of the novel fractal-fractional NMIBC model, based on the original integer-order system. We also detail the model parameters and assumptions. Section 3 provides the essential mathematical preliminaries, including the definitions of the fractal-fractional operators and supporting lemmas. In Section 4, we conduct a thorough qualitative analysis, establishing the existence, uniqueness, positivity, and boundedness of the model's solutions. Section 5 is dedicated to stability analysis, where we compute the basic reproduction number ($\mathcal{R}_0$) and analyze the local and global stability of the disease-free and endemic equilibrium points. In Section 6, we develop a numerical solution for the FF system using the Adomian decomposition transform method (FF-ADM). Section 7 presents a numerical comparison of our chosen method against other schemes and analyzes the convergence rate. Section 8 provides an in-depth discussion of the numerical results, illustrating the dynamic impact of the fractional order α, the fractal dimension β, and key biological parameters. A summary of key findings is presented in a tabular format in Section 9. Section 10 concludes the paper by providing a summary of the work and outlining future research directions.

2. Model formulation

This study develops a new mathematical approach for analyzing the treatment of non-muscle-invasive bladder cancer (NMIBC). The foundation of our work is the integer-order compartmental model introduced by Yosef and Bunimovich-Mendrazitsky [3], which describes the critical interactions

between the intravesical chemotherapy drug Mitomycin C (MMC), the NMIBC tumor cell population, and the responsive effector-immune cells. We first provide a detailed derivation of this base model, followed by its generalization into a fractal-fractional system.

2.1. The base integer-order model

The classical model is structured as a system of three coupled nonlinear ordinary differential equations (ODEs), representing the temporal evolution of the three key populations: $M(t)$, the amount of MMC drug; $T(t)$, the population of tumor cells; and $E(t)$, the population of effector cells.

The rate of change of the MMC drug concentration in the bladder is given by

$$\frac{dM}{dt} = m - \mu_1 M. \tag{2.1}$$

The construction of this equation is based on a simple balance of inflow and outflow. The term m is a constant source term, representing the instillation rate at which the MMC drug is administered into the bladder. The term $-\mu_1 M$ represents the drug's removal from the system. This removal is modeled as a first-order decay process, where μ_1 is the decay rate constant. This constant encapsulates all processes that clear the drug, such as natural chemical decay, absorption by the bladder wall, and dilution.

The dynamics of the tumor cell population are described by the following equation:

$$\frac{dT}{dt} = rT\left(1 - \frac{T}{k}\right) - \frac{p_1 TM}{M + a} - p_2 ET. \tag{2.2}$$

This equation is formulated by considering the factors that contribute to tumor growth and tumor cell death. The first term, $rT(1 - T/k)$, is the logistic growth function. This is a standard assumption in oncology modeling, positing that the tumor cell population T grows at an intrinsic rate r but is limited by the bladder's carrying capacity k. The second term, $-\frac{p_1 TM}{M+a}$, models the targeted killing of tumor cells by the MMC drug. This interaction is represented by Michaelis-Menten kinetics (or a Holling type II functional response), where p_1 is the maximum kill rate and a is the half-saturation constant. This functional form realistically captures a saturation effect: At high drug concentrations ($M \gg a$), the kill rate approaches its maximum, $p_1 T$. The final term, $-p_2 ET$, represents the killing of tumor cells by the immune system. This is modeled as a mass-action or Lotka-Volterra-type interaction, where the rate of predation is proportional to the product of the effector cell population E and the tumor cell population T, governed by the rate constant p_2.

Finally, the rate of change of the effector-immune cell population is given by

$$\frac{dE}{dt} = d_0 + \frac{\gamma p_1 TM}{M + a} - E(p_3 T + \mu_2). \tag{2.3}$$

This equation balances the production, activation, and decay of effector cells. The term d_0 is a constant production rate, representing the basal influx of effector cells from sources like the bone marrow and lymph nodes. The term $\frac{\gamma p_1 TM}{M+a}$ is a critical component linking the chemotherapy to the immune response. It is assumed that the killing of tumor cells by MMC (at the rate $\frac{p_1 TM}{M+a}$) leads to the release of tumor-associated antigens (TAAs). These antigens, in turn, stimulate the recruitment and activation of additional effector cells. This stimulation is modeled as being proportional to the rate of chemotherapy-induced cell death, scaled by an activation coefficient γ. The final term, $-E(p_3 T + \mu_2)$, represents the

removal of effector cells from the system. This removal has two components: $-\mu_2 E$ is the natural death rate of effector cells, and $-p_3 ET$ models the deactivation or exhaustion of effector cells resulting from prolonged interaction with the tumor cells.

2.2. Model assumptions and parameters

The formulation of this model relies on several key biological assumptions. It is assumed that all populations (drug, tumor cells, immune cells) are well-mixed within the bladder compartment. The parameters of the model are considered constant over the simulation period. The logistic growth of the tumor assumes a homogeneous cell population. The immune response is simplified to a single representative population of "effector cells" (e.g., NK cells, CD8+ T cells).

All model parameters are non-negative. Their descriptions, baseline values, and units, as sourced from the foundational study [3] and its cited clinical/experimental literature, are provided in Table 1.

The parameters α and β, summarized in Table 2, respectively represent immune memory effects and tumor microenvironment heterogeneity.

2.3. Model flow diagram

The complex interactions described by the ODE system (2.1)–(2.3) are visualized in the schematic diagram in Figure 1. This diagram illustrates the flow of populations and the network of influences, such as stimulation, inhibition, and decay, that govern the system's dynamics.

Table 1. Model parameters, descriptions, and baseline values [3].

Param.	Description	Baseline Value	Unit
m	Instillation rate of MMC	6.561	μM/day
μ_1	Decay rate of MMC	21.05	day^{-1}
r	Proliferation rate of tumor cells (T)	0.045	day^{-1}
k	Carrying capacity of tumor cells (T)	1×10^9	cells
p_1	Inhibition rate of (T) by MMC	0.2	day^{-1}
a	Half-saturation constant for MMC	100	μM
p_2	Inhibition rate of (T) by (E) cells	3.7×10^{-6}	cells^{-1}day^{-1}
d_0	Production rate of effector cells (E)	1.032×10^5	cells/day
γ	Activation rate of (E) cells	9.12	(unitless)
μ_2	Natural death rate of (E) cells	0.12	day^{-1}
p_3	Deactivation rate of (E) by (T) cells	1.1×10^{-6}	cells^{-1}day^{-1}

Table 2. Model parameters and their biological interpretations, including fractal-fractional parameters.

Parameter	Mathematical Role	Biological Interpretation
$\alpha \in (0, 1]$	Fractional order	Immune memory and delayed treatment response
$\beta \in (0, 1]$	Fractal dimension	Tissue heterogeneity and tumor microenvironment complexity
m	Drug input rate	MMC instillation rate
μ_1	Drug decay rate	MMC clearance from bladder
r	Growth rate	Tumor cell proliferation rate
k	Carrying capacity	Maximum tumor burden
p_1	Drug efficacy	Chemotherapy-induced tumor killing
p_2	Immune efficacy	Effector cell–mediated tumor killing
d_0	Immune source	Basal effector cell production
μ_2	Immune decay	Natural effector cell death
p_3	Immune exhaustion	Tumor-induced effector deactivation

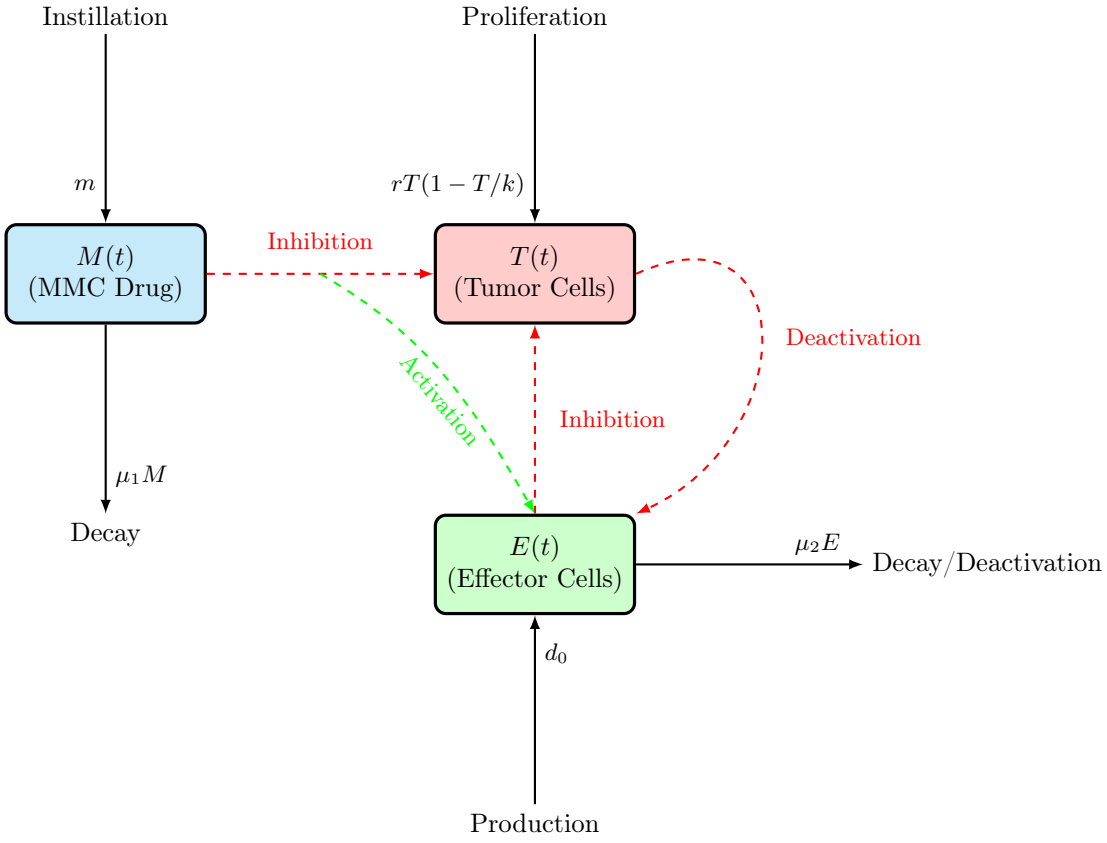

Figure 1. A flow diagram of the NMIBC chemo-immune model. The nodes $M(t)$, $T(t)$, and $E(t)$ are colored blue, red, and green, respectively. Solid arrows represent the flow of populations (production, decay), while dashed arrows represent influence or interaction (inhibition, activation).

2.4. The new fractal-fractional model

The classical integer-order derivative $\frac{d}{dt}$ operates on a local-in-time basis, implying that the future state of the system depends only on its present state. This is a significant simplification, as biological processes are well-known to exhibit memory effects (e.g., the time lag in immune cell activation) and occur in environments that are geometrically complex [10, 11]. Tumor microenvironments, in particular, are not simple Euclidean spaces, but are characterized by fractal-like structures, which inherently affect the diffusion of drugs and the migration of cells [7, 21].

To construct a more realistic and flexible model, we replace the integer-order derivative with a modern fractal-fractional (FF) operator. We employ the FF derivative in the Caputo sense, denoted ${}^{\mathrm{C}}D_t^{\alpha,\beta}$, which is defined by two parameters: the fractional order $0 < \alpha \leq 1$ and the fractal dimension $0 < \beta \leq 1$. The parameter α captures the long-range memory effects of the system, while β accounts for the fractal nature of the underlying medium. The formal definition of this operator is provided in Section 3.

By applying this operator to the left-hand side of the base model (2.1)–(2.3), we formulate the new fractal-fractional NMIBC (FF-NMIBC) model as

$$
\begin{aligned}
{}^{\mathrm{C}}D_t^{\alpha,\beta}M(t) &= m - \mu_1 M(t) && \text{(2.4a)}\\
{}^{\mathrm{C}}D_t^{\alpha,\beta}T(t) &= rT(t)\left(1 - \frac{T(t)}{k}\right) - \frac{p_1 T(t)M(t)}{M(t)+a} \\
&\quad - p_2 E(t)T(t) && \text{(2.4b)}\\
{}^{\mathrm{C}}D_t^{\alpha,\beta}E(t) &= d_0 + \frac{\gamma p_1 T(t)M(t)}{M(t)+a} \\
&\quad - E(t)(p_3 T(t) + \mu_2). && \text{(2.4c)}
\end{aligned}
$$

This system is subject to the initial conditions $M(0) = M_0 \geq 0$, $T(0) = T_0 \geq 0$, and $E(0) = E_0 \geq 0$. This generalized model provides a much richer working for analysis. It is important to note that when $\alpha \to 1$ and $\beta \to 1$, our FF-NMIBC model (2.4) converges exactly to the original integer-order system (2.1)–(2.3). This allows for a direct comparison of the dynamics and highlights the influence of the memory and fractal parameters.

2.5. Biological interpretation of the fractal-fractional operator

The fractal-fractional (FF) operator employed in this study incorporates two independent mechanisms that are relevant to tumor-immune dynamics: Temporal memory and spatial complexity. These effects are governed by the fractional order α and the fractal dimension parameter β, respectively.

The parameter $\alpha \in (0, 1]$ introduces temporal non-locality through the fractional kernel, accounting for immune memory and delayed biological responses. In contrast, the fractal parameter $\beta \in (0, 1]$ scales the time metric as t^β, reflecting the underlying fractal geometry of the tumor microenvironment. This scaling modifies the effective time evolution of the system and is commonly associated with sub-diffusive transport in heterogeneous and irregular biological media.

Table 3 shows a biological perspective, the presence of fractal structures in tumor vasculature, and tissue architecture leads to anomalous diffusion of nutrients, immune cells, and chemotherapeutic agents. The parameter β captures this spatial complexity by embedding fractal effects directly into the

kernel of the fractal-fractional operator, thereby influencing the rate and pattern of tumor growth and treatment response.

Table 3. Interpretation of fractal-fractional parameters and their role in the operator kernel.

Parameter	Biological Meaning	Role in FF Operator
α	Memory effect	Introduces temporal non-locality via fractional kernel
β	Fractal geometry	Scales time as t^β, modeling sub-diffusion

3. Preliminaries

This section provides the essential mathematical definitions and theoretical foundations required for the rigorous analysis of the fractal-fractional NMIBC model. We review the core concepts of fractal-fractional operators, the fixed-point theorems for qualitative analysis, stability criteria for fractional systems, and the foundational principles of the numerical method.

3.1. Fractal-fractional calculus

We begin by defining the operators used to construct the model.

Definition 3.1 (Caputo Fractional Derivative [17,18])**.** *Let $f(t) \in C^n[0,T]$ for some $T > 0$. The Caputo fractional derivative of order α is defined as*

$$ {}^{C}D_t^{\alpha} f(t) = \frac{1}{\Gamma(n-\alpha)} \int_0^t (t-\tau)^{n-\alpha-1} f^{(n)}(\tau) d\tau \tag{3.1} $$

where $n = \lceil \alpha \rceil$ and $\Gamma(\cdot)$ is the Euler Gamma function. For the scope of this paper, we consider $0 < \alpha \leq 1$, which implies $n = 1$.

Definition 3.2 (Fractal Derivative [42])**.** *Let $f(t)$ be a continuous function. Its fractal derivative of order β is defined as*

$$ D_t^{\beta} f(t) = \lim_{\tau \to t} \frac{f(\tau) - f(t)}{\tau^\beta - t^\beta}. \tag{3.2} $$

If $f(t)$ is differentiable on the interval, this derivative is equivalent to

$$ D_t^{\beta} f(t) = \frac{1}{\beta t^{\beta-1}} \frac{df(t)}{dt}, \quad \text{for } t > 0 \tag{3.3} $$

where $0 < \beta \leq 1$. Note that as $\beta \to 1$, $D_t^\beta f(t)$ converges to the standard first derivative $\frac{df(t)}{dt}$.

Definition 3.3 (Caputo-type Fractal-Fractional (FF) Derivative [36,37])**.** *Let $f(t)$ be a continuous and differentiable function on $(0,T)$. The fractal-fractional derivative in the Caputo sense, with a power-law kernel, is defined by combining the Caputo derivative and the fractal derivative:*

$$ {}^{C}D_t^{\alpha,\beta} f(t) = \frac{1}{\Gamma(1-\alpha)} \int_0^t (t-\tau)^{-\alpha} D_\tau^{\beta} f(\tau) d\tau \tag{3.4} $$

where $0 < \alpha \leq 1$, $0 < \beta \leq 1$. By substituting the definition of $D_\tau^\beta f(\tau)$, we get the explicit form

$$ {}^{C}D_t^{\alpha,\beta} f(t) = \frac{1}{\Gamma(1-\alpha)} \int_0^t (t-\tau)^{-\alpha} \left(\frac{1}{\beta \tau^{\beta-1}} \frac{df(\tau)}{d\tau} \right) d\tau. \tag{3.5} $$

Definition 3.4 (Fractal-Fractional Integral [36]). *The corresponding fractal-fractional integral operator with a power-law kernel, which serves as the inverse operator, is defined as*

$$^{FF}I_t^{\alpha,\beta} f(t) = \frac{\beta}{\Gamma(\alpha)} \int_0^t \tau^{\beta-1}(t^\beta - \tau^\beta)^{\alpha-1} f(\tau) d\tau. \tag{3.6}$$

3.2. Foundations for qualitative analysis

To analyze the existence and uniqueness of the solutions for the FF-NMIBC model, we rely on fixed-point theory. The following lemma is crucial as it transforms the differential system into an equivalent integral system.

Lemma 3.5 ([21, 36]). *The fractal-fractional initial value problem*

$$^{C}D_t^{\alpha,\beta} u(t) = f(t, u(t)), \quad u(0) = u_0,$$

where $^{C}D_t^{\alpha,\beta}$ is the Caputo-type FF derivative, can be reformulated as the following nonlinear Volterra-type integral equation:

$$u(t) = u_0 + \frac{\beta}{\Gamma(\alpha)} \int_0^t \tau^{\beta-1}(t^\beta - \tau^\beta)^{\alpha-1} f(\tau, u(\tau)) d\tau. \tag{3.7}$$

Proof. The proof is obtained by applying the fractal-fractional integral operator $^{FF}I_t^{\alpha,\beta}$ to both sides of the differential equation and using the property that $^{FF}I_t^{\alpha,\beta}(^{C}D_t^{\alpha,\beta} u(t)) = u(t) - u(0)$. □

This lemma allows us to define an operator on a complete metric space and apply the Banach fixed-point theorem to prove the existence of a unique solution.

Theorem 3.6 (Banach Fixed-Point Theorem [43,44]). *Let (X, d) be a non-empty complete metric space. Let $T : X \to X$ be a mapping such that for all $x, y \in X$, there exists a constant $0 \leq K < 1$, for which*

$$d(T(x), T(y)) \leq K d(x, y).$$

Then, T is a contraction mapping and admits a unique fixed-point x^* in X (that is, $T(x^*) = x^*$).

3.3. Foundations for stability analysis

The stability analysis of fractional-order systems differs significantly from that of integer-order systems. The stability is determined not just by the sign of the real parts of the eigenvalues, but by their location in the complex plane relative to a sector defined by the fractional order α.

Theorem 3.7 (Matignon's Theorem [45,46]). *Consider the linear fractional-order autonomous system $^{C}D_t^{\alpha}\mathbf{x} = \mathbf{J}\mathbf{x}$, where $\mathbf{x} \in \mathbb{R}^n$, $0 < \alpha \leq 1$, and $\mathbf{J}$ is the $n \times n$ Jacobian matrix. The disease-free equilibrium point at the origin is locally asymptotically stable if and only if all eigenvalues λ_i of the matrix $\mathbf{J}$ satisfy the condition*

$$|\arg(\lambda_i)| > \frac{\alpha\pi}{2}. \tag{3.8}$$

This implies that for $\alpha \in (0, 1)$, stability is maintained even if some eigenvalues have a positive real part, provided they lie outside the wedge defined by $\frac{\alpha\pi}{2}$. For $\alpha = 1$, this condition reduces to the classical Routh-Hurwitz criterion, $Re(\lambda_i) < 0$.

For global stability, we employ the Lyapunov direct method, adapted for fractional-order derivatives.

Remark 3.8. *For the fractal–fractional system considered in this work, the local stability conditions derived from the Jacobian matrix are interpreted through Matignon's theorem. In particular, for* $0 < \alpha \leq 1$*, an equilibrium point is locally asymptotically stable if and only if all eigenvalues* λ_i *of the Jacobian satisfy*

$$|\arg(\lambda_i)| > \frac{\alpha\pi}{2}.$$

Throughout Section 5, the fractional Routh–Hurwitz conditions are used to verify that this criterion is fulfilled.

Lemma 3.9 (Fractional Lyapunov Stability [47, 48])**.** *Let* $\mathbf{x} = \mathbf{0}$ *be an equilibrium point for the system* ${}^{C}D_t^{\alpha}\mathbf{x}(t) = \mathbf{f}(\mathbf{x}(t))$*. Let* $V(\mathbf{x}(t))$ *be a continuously differentiable, positive definite, scalar function (a Lyapunov function) defined on a domain* Ω *containing the origin. If the fractional derivative of* V *satisfies* ${}^{C}D_t^{\alpha}V(\mathbf{x}(t)) \leq 0$ *for all* $\mathbf{x} \in \Omega$*, then the equilibrium point is stable in the sense of Lyapunov. If* ${}^{C}D_t^{\alpha}V(\mathbf{x}(t)) < 0$*, the equilibrium point is asymptotically stable. This result is extended to fractal-fractional operators* ${}^{C}D_t^{\alpha,\beta}$ *by noting that the sign of* ${}^{C}D_t^{\alpha,\beta}V(\mathbf{x}(t))$ *is determined by the sign of* $\frac{dV}{dt}$*.*

3.4. Preliminaries for the numerical method

The numerical solution is constructed using the Adomian decomposition transform method. This method combines an integral transform (such as Laplace, Sumudu, etc.) with the Adomian decomposition.

Definition 3.10 (Adomian decomposition method (ADM) [49])**.** *Consider a nonlinear functional equation* $u = N(u) + g$*, where* N *is a nonlinear operator and* g *is a known function. The ADM seeks a solution in the form of an infinite series:*

$$u(t) = \sum_{n=0}^{\infty} u_n(t). \tag{3.9}$$

The nonlinear term $N(u)$ *is likewise decomposed into an infinite series of polynomials* A_n*, known as Adomian polynomials:*

$$N(u) = \sum_{n=0}^{\infty} A_n(u_0, u_1, \ldots, u_n). \tag{3.10}$$

Definition 3.11 (Adomian Polynomials [50])**.** *The Adomian polynomials* A_n *are generated for any form of nonlinearity using the formula*

$$A_n = \frac{1}{n!}\left[\frac{d^n}{d\lambda^n}N\left(\sum_{i=0}^{\infty}\lambda^i u_i\right)\right]_{\lambda=0}, \quad n = 0, 1, 2, \ldots \tag{3.11}$$

For example, the first few polynomials are $A_0 = N(u_0)$*,* $A_1 = u_1N'(u_0)$*,* $A_2 = u_2N'(u_0) + \frac{u_1^2}{2!}N''(u_0)$*, and so on.*

The ADM [51, 52] applies the Laplace transform $\mathcal{G}[\cdot]$ to the differential equation, which simplifies the derivative and converts the problem into an algebraic one.

Lemma 3.12 (Laplace Transform of Caputo Derivative [18]). *The Laplace Transform, denoted $\mathcal{L}[\cdot]$, when applied to the Caputo fractional derivative of order $0 < \alpha \leq 1$, is given by*

$$\mathcal{L}\left[{}^{C}D_t^{\alpha} f(t)\right](s) = s^{\alpha}\mathcal{L}[f(t)](s) - s^{\alpha-1}f(0). \tag{3.12}$$

This property is fundamental in isolating the transformed function $\mathcal{L}[f(t)](s)$, to which the Adomian decomposition is then applied. The methodology for adapting this to the FF operator ${}^{C}D_t^{\alpha,\beta}$ will be detailed in Section 6.

4. Qualitative analysis

In this section, we establish the fundamental mathematical properties of the proposed fractal-fractional NMIBC model (2.4). We will prove the existence and uniqueness of the solutions, demonstrate that the solutions are non-negative for all time (positivity), and show that they are bounded. These properties are essential for ensuring the model is mathematically well-posed and biologically realistic.

4.1. Existence and uniqueness

To prove the existence and uniqueness of the solution for system (2.4), we utilize the Banach fixed-point theorem (Theorem 3.6) on a complete metric space. We first reformulate the system of differential equations as a system of Volterra-type integral equations using Lemma 3.5.

Let $\Psi(t) = (M(t), T(t), E(t))^T$. The FF-NMIBC system (2.4) can be written in the general form

$${}^{C}D_t^{\alpha,\beta}\Psi(t) = \mathcal{F}(t, \Psi(t)), \quad \Psi(0) = \Psi_0 \tag{4.1}$$

where $\Psi_0 = (M_0, T_0, E_0)^T$ and $\mathcal{F}$ is a vector-valued function with components

$$\mathcal{F}_1(t, \Psi(t)) = m - \mu_1 M(t) \tag{4.2a}$$

$$\mathcal{F}_2(t, \Psi(t)) = rT(t)\left(1 - \frac{T(t)}{k}\right) - \frac{p_1 T(t)M(t)}{M(t) + a} - p_2 E(t)T(t) \tag{4.2b}$$

$$\mathcal{F}_3(t, \Psi(t)) = d_0 + \frac{\gamma p_1 T(t)M(t)}{M(t) + a} - E(t)(p_3 T(t) + \mu_2). \tag{4.2c}$$

Using Lemma 3.5, this initial value problem is equivalent to the following integral system:

$$\Psi(t) = \Psi_0 + \frac{\beta}{\Gamma(\alpha)}\int_0^t \tau^{\beta-1}(t^{\beta} - \tau^{\beta})^{\alpha-1}\mathcal{F}(\tau, \Psi(\tau))d\tau. \tag{4.3}$$

We now show that the kernels $\mathcal{F}_i$ satisfy the Lipschitz condition, which is a prerequisite for applying the Banach fixed-point theorem.

Lemma 4.1. *Let $\mathcal{E} = C([0, T]; \mathbb{R}^3)$ denote the Banach space of continuous vector-valued functions on $[0, T]$. We equip E with the norm*

$$\|\mathbf{U}\| = \sup_{t\in[0,T]} \left(|M(t)| + |T(t)| + |E(t)|\right), \tag{4.4}$$

where $\mathbf{U}(t) = (M(t), T(t), E(t))^{\top}$. Then, $(\mathcal{E}, \|\cdot\|)$ is a complete normed linear space.

Lemma 4.2 (Lipschitz Condition)**.** *The kernels $\mathcal{F}_i(t, \Psi(t))$ for $i = 1, 2, 3$ satisfy the Lipschitz condition with respect to Ψ in a bounded domain.*

Proof. Let $\Psi(t) = (M, T, E)^T$ and $\bar{\Psi}(t) = (\bar{M}, \bar{T}, \bar{E})^T$ be two distinct solution vectors. We consider a time interval $[0, \mathcal{T}]$ where $0 < \mathcal{T} < \infty$. We assume the solutions are bounded in this interval, such that $M, \bar{M} \leq C_M$, $T, \bar{T} \leq C_T$, and $E, \bar{E} \leq C_E$ for some positive constants C_M, C_T, C_E.

First, for $\mathcal{F}_1$,

$$\begin{aligned} \|\mathcal{F}_1(\Psi) - \mathcal{F}_1(\bar{\Psi})\| &= \|(m - \mu_1 M) - (m - \mu_1 \bar{M})\| \\ &= \mu_1 \|M - \bar{M}\| \\ &\leq \mu_1 \|M - \bar{M}\| + 0\|T - \bar{T}\| + 0\|E - \bar{E}\| \\ &\leq L_1 \|\Psi - \bar{\Psi}\|, \quad \text{with } L_1 = \mu_1. \end{aligned}$$

Second, for $\mathcal{F}_2$,

$$\begin{aligned} &\|\mathcal{F}_2(\Psi) - \mathcal{F}_2(\bar{\Psi})\| = \\ &\left\| \left[rT - \frac{rT^2}{k} - \frac{p_1 TM}{M + a} - p_2 ET \right] \right. \\ &\left. - \left[r\bar{T} - \frac{r\bar{T}^2}{k} - \frac{p_1 \bar{T}\bar{M}}{\bar{M} + a} - p_2 \bar{E}\bar{T} \right] \right\| \\ &\leq r\|T - \bar{T}\| + \frac{r}{k}\|T^2 - \bar{T}^2\| + p_1 \left\| \frac{TM}{M + a} - \frac{\bar{T}\bar{M}}{\bar{M} + a} \right\| \\ &\quad + p_2 \|ET - \bar{E}\bar{T}\|. \end{aligned}$$

We bound each term. $\|T^2 - \bar{T}^2\| = \|(T + \bar{T})(T - \bar{T})\| \leq (C_T + C_T)\|T - \bar{T}\| = 2C_T\|T - \bar{T}\|$.
The term $\|ET - \bar{E}\bar{T}\| = \|ET - E\bar{T} + E\bar{T} - \bar{E}\bar{T}\| \leq C_E\|T - \bar{T}\| + C_T\|E - \bar{E}\|$.
The Michaelis-Menten term is also Lipschitz in a bounded domain. The partial derivative with respect to T is $\frac{p_1 M}{M+a} \leq p_1$, and with respect to M is $\frac{p_1 Ta}{(M+a)^2} \leq \frac{p_1 C_T a}{a^2} = \frac{p_1 C_T}{a}$.
Combining these, we find constants k_M, k_T, k_E such that

$$\|\mathcal{F}_2(\Psi) - \mathcal{F}_2(\bar{\Psi})\| \leq k_M\|M - \bar{M}\| + k_T\|T - \bar{T}\| + k_E\|E - \bar{E}\|.$$

Thus, $\|\mathcal{F}_2(\Psi) - \mathcal{F}_2(\bar{\Psi})\| \leq L_2\|\Psi - \bar{\Psi}\|$, where $L_2 = \max(k_M, k_T, k_E)$.

Third, for $\mathcal{F}_3$, the logic is identical. The term $\frac{\gamma p_1 TM}{M+a}$ is Lipschitz, as is $E(p_3 T + \mu_2)$. Therefore, we can find a constant L_3 such that $\|\mathcal{F}_3(\Psi) - \mathcal{F}_3(\bar{\Psi})\| \leq L_3\|\Psi - \bar{\Psi}\|$.
Finally, by letting $\mathcal{L} = \max(L_1, L_2, L_3)$, we have

$$\|\mathcal{F}(t, \Psi) - \mathcal{F}(t, \bar{\Psi})\| \leq \mathcal{L}\|\Psi - \bar{\Psi}\|. \tag{4.5}$$

This confirms that the kernel vector $\mathcal{F}$ satisfies the Lipschitz condition. □

Theorem 4.3 (Existence and Uniqueness)**.** *For a finite-time interval $[0, \mathcal{T}]$, a unique solution $\Psi(t)$ for the fractal-fractional NMIBC model (2.4) with initial conditions Ψ_0 exists.*

Proof. Let $X = C([0, \mathcal{T}], \mathbb{R}^3)$ be the Banach space of all continuous vector-valued functions on $[0, \mathcal{T}]$ equipped with the supremum norm $\|\Psi\|_\infty = \sup_{t\in[0,\mathcal{T}]} \|\Psi(t)\|$. We define a Picard-type operator $\mathcal{P} : X \to X$ based on the integral equation (4.3):

$$(\mathcal{P}\Psi)(t) = \Psi_0 + \frac{\beta}{\Gamma(\alpha)} \int_0^t \tau^{\beta-1}(t^\beta - \tau^\beta)^{\alpha-1}\mathcal{F}(\tau, \Psi(\tau))d\tau. \tag{4.6}$$

The existence of a unique solution $\Psi(t)$ is equivalent to the existence of a unique fixed point for the operator $\mathcal{P}$. We will now show that $\mathcal{P}$ is a contraction mapping.
Consider two functions $\Psi, \bar{\Psi} \in X$.

$$\begin{aligned}
&\|(\mathcal{P}\Psi)(t) - (\mathcal{P}\bar{\Psi})(t)\| = \\
&\left\| \frac{\beta}{\Gamma(\alpha)} \int_0^t \tau^{\beta-1}(t^\beta - \tau^\beta)^{\alpha-1}(\mathcal{F}(\tau, \Psi) - \mathcal{F}(\tau, \bar{\Psi}))d\tau \right\| \\
&\leq \frac{\beta}{\Gamma(\alpha)} \int_0^t \tau^{\beta-1}(t^\beta - \tau^\beta)^{\alpha-1}\|\mathcal{F}(\tau, \Psi) - \mathcal{F}(\tau, \bar{\Psi})\|d\tau.
\end{aligned}$$

Using the Lipschitz condition from Lemma 4.2,

$$\begin{aligned}
&\|(\mathcal{P}\Psi)(t) - (\mathcal{P}\bar{\Psi})(t)\| \\
&\leq \frac{\beta\mathcal{L}}{\Gamma(\alpha)} \int_0^t \tau^{\beta-1}(t^\beta - \tau^\beta)^{\alpha-1}\|\Psi(\tau) - \bar{\Psi}(\tau)\|d\tau \\
&\leq \frac{\beta\mathcal{L}}{\Gamma(\alpha)}\|\Psi - \bar{\Psi}\|_\infty \int_0^t \tau^{\beta-1}(t^\beta - \tau^\beta)^{\alpha-1}d\tau.
\end{aligned}$$

Let us evaluate the integral. We use the substitution $u = \tau^\beta$, so $du = \beta\tau^{\beta-1}d\tau$.

$$\begin{aligned}
\int_0^t \tau^{\beta-1}(t^\beta - \tau^\beta)^{\alpha-1}d\tau &= \frac{1}{\beta}\int_0^{t^\beta} (t^\beta - u)^{\alpha-1}du \\
&= \frac{1}{\beta}\left[-\frac{(t^\beta - u)^\alpha}{\alpha}\right]_0^{t^\beta} \\
&= \frac{1}{\beta\alpha}(t^\beta)^\alpha = \frac{t^{\alpha\beta}}{\alpha\beta}.
\end{aligned}$$

Substituting this back, we have

$$\|(\mathcal{P}\Psi)(t) - (\mathcal{P}\bar{\Psi})(t)\| \leq \frac{\beta\mathcal{L}}{\Gamma(\alpha)}\frac{t^{\alpha\beta}}{\alpha\beta}\|\Psi - \bar{\Psi}\|_\infty.$$

Using the property $\Gamma(\alpha + 1) = \alpha\Gamma(\alpha)$,

$$\|(\mathcal{P}\Psi)(t) - (\mathcal{P}\bar{\Psi})(t)\| \leq \frac{\mathcal{L}t^{\alpha\beta}}{\Gamma(\alpha + 1)}\|\Psi - \bar{\Psi}\|_\infty.$$

By taking the supremum over $t \in [0, \mathcal{T}]$,

$$\|(\mathcal{P}\Psi) - (\mathcal{P}\bar{\Psi})\|_\infty \leq \frac{\mathcal{L}\mathcal{T}^{\alpha\beta}}{\Gamma(\alpha + 1)}\|\Psi - \bar{\Psi}\|_\infty.$$

We can define $K = \frac{\mathcal{L}\mathcal{T}^{\alpha\beta}}{\Gamma(\alpha+1)}$. The operator $\mathcal{P}$ is a contraction mapping if $K < 1$. Since $\mathcal{L}$, α, and β are fixed, we can always choose a time $\mathcal{T}$ sufficiently small such that $\mathcal{T}^{\alpha\beta} < \Gamma(\alpha+1)/\mathcal{L}$. Therefore, on the interval $[0, \mathcal{T}]$, the operator $\mathcal{P}$ is a contraction. By the Banach fixed-point theorem, $\mathcal{P}$ admits a unique fixed point, which corresponds to the unique local solution of the FF-NMIBC model. This local solution can be extended to a maximal interval of existence. □

Note: Extension to a maximal interval Let $T_{\max} = \sup\{T > 0 : \Psi(t) \text{ exists uniquely on } [0, T]\}$. Since $F(t, \Psi)$ is locally Lipschitz in Ψ (Lemma 4.2) and continuous in t, the solution can be continued as long as it remains bounded.
More precisely, if $T_{\max} < \infty$ and $\sup_{t\in[0,T_{\max})} \|\Psi(t)\| < \infty$, then $\Psi(T_{\max} - \varepsilon)$ lies in a bounded set where the Lipschitz constant is finite, and the same contraction argument used above yields existence on $[T_{\max} - \varepsilon, T_{\max} - \varepsilon + \delta]$, contradicting the definition of $T_{\max}$.
Hence, either $T_{\max} = \infty$ or $\|\Psi(t)\| \to \infty$ as $t \to T_{\max}^-$, which justifies the extension to a maximal interval of existence.

4.2. Nonnegativity of solutions

For the model to be biologically meaningful, all state variables must remain non-negative for all $t \geq 0$, given non-negative initial conditions. We establish this in the following theorem.

Theorem 4.4 (Nonnegativity)**.** *Let the initial conditions be* $\Psi_0 = (M(0), T(0), E(0)) \in \mathbb{R}^3_+ = \{(x, y, z) \in \mathbb{R}^3 : x \geq 0, y \geq 0, z \geq 0\}$. *Then, the solution* $\Psi(t) = (M(t), T(t), E(t))$ *of system (2.4) remains nonnegative for all* $t \geq 0$.

Proof. We will prove the non-negativity of each compartment by analyzing the vector field on the boundaries of the positive octant $\mathbb{R}^3_+$.
First, consider the $M(t)$ compartment. We want to show that if $M(0) \geq 0$, then $M(t) \geq 0$ for all $t > 0$. Let us examine the solution at the point where it might cross the boundary, i.e., $M(t) = 0$.

$$ {}^{\mathrm{C}}D_t^{\alpha,\beta} M(t)\Big|_{M=0} = m - \mu_1(0) = m. $$

Since $m > 0$, the vector field on the plane $M = 0$ points strictly into the positive octant. The fractal-fractional derivative at $M = 0$ is positive, implying that the function $M(t)$ cannot cross from positive to negative. A formal proof can be based on the fractional equivalent of Nagumo's theorem [21]. From the integral formulation (3.7), if $M(t_1) = 0$ for some $t_1 > 0$, the kernel $\mathcal{F}_1(\tau, \Psi(\tau)) \geq m - \mu_1 M(\tau)$. If $M(\tau)$ is small, $\mathcal{F}_1$ is positive. Thus, $M(t)$ is non-decreasing from $M = 0$. Therefore, $M(t) \geq 0$.
Second, consider the $T(t)$ compartment. On the boundary $T = 0$,

$$ \begin{aligned} {}^{\mathrm{C}}D_t^{\alpha,\beta} T(t)\Big|_{T=0} &= r(0)\left(1 - \frac{0}{k}\right) - \frac{p_1(0)M}{M+a} - p_2 E(0) \\ &= 0. \end{aligned} $$

This indicates that the $T = 0$ plane is an invariant manifold. To show that solutions starting with $T(0) > 0$ remain positive, we can rewrite the T equation as

$$ {}^{\mathrm{C}}D_t^{\alpha,\beta} T(t) = T\left[r\left(1 - \frac{T}{k}\right) - \frac{p_1 M}{M+a} - p_2 E\right] $$

$$= T \cdot G(M, T, E).$$

The solution to this (in its fractional integral form) can be shown to be $T(t) \geq T(0)\mathcal{E}(t)$, where $\mathcal{E}(t) > 0$ is a function related to the Mittag-Leffler function. As $T(0) \geq 0$, it follows that $T(t) \geq 0$ for all $t \geq 0$. Third, consider the $E(t)$ compartment. On the boundary $E = 0$,

$$\begin{aligned} {}^{\mathrm{C}}D_t^{\alpha,\beta}E(t)\Big|_{E=0} &= d_0 + \frac{\gamma p_1 T M}{M + a} - (0)(p_3 T + \mu_2) \\ &= d_0 + \frac{\gamma p_1 T M}{M + a}. \end{aligned}$$

Since $d_0 > 0$, $p_1 > 0$, $\gamma > 0$, and we have already established $T(t) \geq 0$ and $M(t) \geq 0$, we have:

$${}^{\mathrm{C}}D_t^{\alpha,\beta}E(t)\Big|_{E=0} \geq d_0 > 0.$$

The vector field on the plane $E = 0$ (where $T \geq 0, M \geq 0$) points strictly into the positive octant. Thus, any solution starting with $E(0) \geq 0$ will remain non-negative for all $t \geq 0$.
Since all compartments are non-negative, the positive octant $\mathbb{R}^3_+$ is a positively invariant region for system (2.4). □

Remark. In this work, "nonnegativity" means $M(t), T(t), E(t) \geq 0$ for all $t \geq 0$. The term "positivity" is sometimes used in the biological modeling literature in the same sense; however, mathematically, the result establishes nonnegativity (invariance of $\mathbb{R}^3_+$).

4.3. Boundedness of solutions

We now demonstrate that all solutions of the FF-NMIBC model that start in the positive octant $\mathbb{R}^3_+$ are bounded.

Theorem 4.5 (Boundedness)**.** *All solutions $\Psi(t) = (M(t), T(t), E(t))$ of system (2.4) that start in $\mathbb{R}^3_+$ are bounded.*

Proof. We prove the boundedness of each component.

For $M(t)$: The first equation is ${}^{\mathrm{C}}D_t^{\alpha,\beta}M(t) = m - \mu_1 M(t)$. This is a linear FF differential equation. The equilibrium point is $M^* = m/\mu_1$. If $M(t) > M^*$, then $m - \mu_1 M(t) < 0$. This implies that ${}^{\mathrm{C}}D_t^{\alpha,\beta}M(t) < 0$, and the function $M(t)$ will decrease. By the generalized fractional comparison principle [47, 48], the solution $M(t)$ is asymptotically stable toward M^*. Therefore, $M(t)$ is bounded. Any solution starting at $M(0)$ will tend towards m/μ_1, and $M(t) \leq \max(M(0), m/\mu_1) = K_M$.

For $T(t)$: From the second equation, and using the fact that $M(t), E(t), p_1, p_2 \geq 0$,

$$\begin{aligned} {}^{\mathrm{C}}D_t^{\alpha,\beta}T(t) &= rT\left(1 - \frac{T}{k}\right) - \frac{p_1 T M}{M + a} - p_2 E T \\ &\leq rT\left(1 - \frac{T}{k}\right). \end{aligned}$$

This means the tumor growth is, at most, logistic. By the fractional comparison principle, if $T(t) > k$, then $1 - T(t)/k < 0$, which implies ${}^{\mathrm{C}}D_t^{\alpha,\beta}T(t) < 0$. The function $T(t)$ will decrease. Thus, $T(t)$ is bounded by $K_T = \max(T(0), k)$.

For $E(t)$: From the third equation, we use the bounds K_M and K_T that we just found.

$$\begin{aligned} {}^{\mathrm{C}}D_t^{\alpha,\beta}E(t) &= d_0 + \frac{\gamma p_1 T M}{M+a} - E(p_3 T + \mu_2) \\ &\leq d_0 + \frac{\gamma p_1 T M}{a} - \mu_2 E \quad (\text{since } M + a \geq a) \\ &\leq d_0 + \frac{\gamma p_1 K_T K_M}{a} - \mu_2 E. \end{aligned}$$

Let $A = d_0 + \frac{\gamma p_1 K_T K_M}{a}$. The constant A is positive and finite. We have

$${}^{\mathrm{C}}D_t^{\alpha,\beta}E(t) \leq A - \mu_2 E.$$

Similar to the $M(t)$ compartment, this is a linear FF inequality. If $E(t) > A/\mu_2$, then $A - \mu_2 E(t) < 0$, which implies ${}^{\mathrm{C}}D_t^{\alpha,\beta}E(t) < 0$. The function $E(t)$ will decrease. Therefore, $E(t)$ is bounded by $K_E = \max(E(0), A/\mu_2)$.

Since $M(t)$, $T(t)$, and $E(t)$ are all bounded, the solution $\Psi(t)$ is bounded for all $t \geq 0$. □

The combination of positivity and boundedness ensures that the solutions are confined to a compact and positively invariant subset $\Omega \subset \mathbb{R}^3_+$, where

$$\Omega = \left\{(M, T, E) \in \mathbb{R}^3_+ : M \leq K_M, T \leq K_T, E \leq K_E\right\}.$$

This establishes that the FF-NMIBC model is mathematically and biologically well-posed.

5. Stability analysis

This section investigates the dynamic stability of the FF-NMIBC model (2.4). We first determine the equilibrium points of the system and derive the basic reproduction number ($\mathcal{R}_0$), which acts as a critical threshold. We then analyze the local stability of these equilibria using the Jacobian matrix in conjunction with fractional stability theory. Finally, we formulate theorems for the global stability of the system.

5.1. Equilibrium points

The equilibrium points (or steady states) of the system are found by setting the time derivatives in (2.4) to zero:

$$m - \mu_1 M = 0 \tag{5.1a}$$

$$T\left[r\left(1 - \frac{T}{k}\right) - \frac{p_1 M}{M+a} - p_2 E\right] = 0 \tag{5.1b}$$

$$d_0 + \frac{\gamma p_1 T M}{M+a} - E(p_3 T + \mu_2) = 0. \tag{5.1c}$$

From (5.1a), the steady-state concentration of the MMC drug is independent of the other compartments:

$$M^* = \frac{m}{\mu_1}.$$

This value M^* will be the same for all equilibrium points. From (5.1b), we have two possible cases for T.

5.1.1. Case 1: Disease-free equilibrium (DFE)

This equilibrium corresponds to the tumor-free state, $T = 0$. We denote this point as $E_0 = (M^*, T_0, E_0)$. Setting $T_0 = 0$ in (5.1c), we get

$$d_0 + 0 - E_0(0 + \mu_2) = 0$$
$$d_0 - \mu_2 E_0 = 0 \implies E_0 = \frac{d_0}{\mu_2}.$$

Thus, the system admits a unique disease-free equilibrium (DFE), given by

$$E_0 = (M^*, T_0, E_0) = \left(\frac{m}{\mu_1}, 0, \frac{d_0}{\mu_2}\right). \tag{5.2}$$

This state represents a successfully treated patient where the tumor is eliminated, and the drug and effector cell populations have stabilized.

5.1.2. Case 2: Endemic (Tumor) equilibrium (EE)

This equilibrium corresponds to the persistence of the tumor, $T \neq 0$. We denote this point as $E^* = (M^*, T^*, E^*)$, where $T^* > 0$. Since $T \neq 0$, we can divide (5.1b) by T to get

$$r\left(1 - \frac{T^*}{k}\right) - \frac{p_1 M^*}{M^* + a} - p_2 E^* = 0. \tag{5.3}$$

For notational convenience, we define the following constants:

$$C_1 = \frac{p_1 a M^*}{(M^* + a)^2}, \qquad C_2 = p_2 E^*, \tag{5.4}$$

which are positive quantities evaluated at the endemic equilibrium (M^*, T^*, E^*).
From (5.1c), we can solve for E^*:

$$E^* = \frac{d_0 + \frac{\gamma p_1 T^* M^*}{M^* + a}}{p_3 T^* + \mu_2}. \tag{5.5}$$

Substituting (5.5) into (5.3) yields a single, complex equation for T^*:

$$r\left(1 - \frac{T^*}{k}\right) - \frac{p_1 M^*}{M^* + a} = p_2\left(\frac{d_0 + \frac{\gamma p_1 T^* M^*}{M^* + a}}{p_3 T^* + \mu_2}\right). \tag{5.6}$$

To simplify, let $C_1 = \frac{p_1 M^*}{M^* + a}$ and $C_2 = \frac{\gamma p_1 M^*}{M^* + a}$.

$$\left[(r - C_1) - \frac{r}{k} T^*\right](p_3 T^* + \mu_2) = p_2(d_0 + C_2 T^*).$$

Expanding and collecting terms in powers of T^* leads to the quadratic equation $A(T^*)^2 + B(T^*) + C = 0$, where:

$$A = \frac{r p_3}{k}$$
$$B = \left(\frac{r\mu_2}{k} + p_2 C_2 - p_3(r - C_1)\right)$$
$$C = p_2 d_0 - \mu_2(r - C_1).$$

Since $A > 0$, the existence of a positive real solution T^* depends on the signs of B and C.

5.2. Basic reproduction number ($\mathcal{R}_0$)

In oncology modeling, the basic reproduction number (or net growth rate) $\mathcal{R}_0$ represents the net reproductive rate of the tumor at the disease-free state. It is a threshold that determines whether the tumor will grow from a small population or be eliminated. The per-capita growth rate of the tumor T at the DFE is

$$\begin{aligned}\frac{1}{T}\cdot{}^{\mathrm{C}}D_t^{\alpha,\beta}T\Big|_{E_0} &= \left[r\left(1-\frac{T}{k}\right)-\frac{p_1M}{M+a}-p_2E\right]\Big|_{E_0}\\ &= r-\frac{p_1M^*}{M^*+a}-p_2E_0.\end{aligned}$$

The tumor grows if this rate is positive and decays if it is negative. The "growth" term is r, and the "decay" terms (at DFE) are the inhibitions from the drug ($p_1M^*/(M^*+a)$) and the immune system (p_2E_0). We define $\mathcal{R}_0$ as the ratio of growth to decay:

$$\mathcal{R}_0 = \frac{r}{\frac{p_1M^*}{M^*+a}+p_2E_0}. \tag{5.7}$$

Substituting the DFE values $M^* = m/\mu_1$ and $E_0 = d_0/\mu_2$,

$$\mathcal{R}_0 = \frac{r}{\frac{p_1(m/\mu_1)}{m/\mu_1+a}+p_2\frac{d_0}{\mu_2}}. \tag{5.8}$$

The DFE E_0 is stable if the net growth rate is negative, which corresponds to $\mathcal{R}_0 < 1$. It is unstable if $\mathcal{R}_0 > 1$.

Now, let's re-examine the coefficient C of the quadratic equation for T^*:

$$\begin{aligned}C &= p_2d_0-\mu_2(r-C_1)\\ &= p_2d_0+\mu_2C_1-r\mu_2\\ &= \mu_2\left(p_2\frac{d_0}{\mu_2}+C_1-r\right)\\ &= \mu_2\left((p_2E_0+C_1)-r\right)\\ &= \mu_2(p_2E_0+C_1)\left(1-\frac{r}{p_2E_0+C_1}\right)\\ C &= \mu_2(p_2E_0+C_1)(1-\mathcal{R}_0).\end{aligned}$$

Since $\mu_2(p_2E_0+C_1) > 0$, the sign of C is determined by $(1-\mathcal{R}_0)$.

If $\mathcal{R}_0 < 1$, then $C > 0$. Since $A > 0$, the quadratic equation can have zero or two positive roots (or two negative roots, depending on B).

If $\mathcal{R}_0 > 1$, then $C < 0$. Since $A > 0$, $C/A < 0$, which is the product of the roots.

This guarantees that the quadratic equation has exactly one positive real root and one negative real root. Therefore, a unique endemic equilibrium E^* exists if and only if $\mathcal{R}_0 > 1$. This indicates a transcritical bifurcation at $\mathcal{R}_0 = 1$.

Remark 5.1 (Biological Interpretation of $\mathcal{R}_0$)**.** *Biologically, the basic reproduction number $\mathcal{R}_0$ represents the ratio of the tumor's proliferation potential to the immune system's clearance capacity.*

The numerator corresponds to the rate of new tumor cell generation, while the denominator aggregates the rates of tumor elimination (natural death and immune-induced killing) at the disease-free equilibrium. Thus, $\mathcal{R}_0 > 1$ implies that tumor cells are generated faster than the immune system can clear them, leading to disease persistence.

5.3. Local stability analysis

We now analyze the local asymptotic stability of the equilibrium points. The stability of a fractal-fractional system ${}^{\mathrm{C}}D_t^{\alpha,\beta}\Psi = \mathcal{F}(\Psi)$ is determined by the eigenvalues λ_i of the Jacobian matrix $\mathbf{J} = \frac{\partial \mathcal{F}}{\partial \Psi}$ evaluated at the equilibrium. Based on Theorem 3.7, the equilibrium is locally asymptotically stable (LAS) if all eigenvalues satisfy $|\arg(\lambda_i)| > \alpha\pi/2$. For $\alpha \in (0, 1]$, this is satisfied if all eigenvalues are in the left-half of the complex plane, $\mathrm{Re}(\lambda_i) < 0$.

The Jacobian matrix for the system $\Psi = (M, T, E)^T$ is

$$\mathbf{J} = \begin{pmatrix} -\mu_1 & 0 & 0 \\ -\frac{p_1 aT}{(M+a)^2} & r - \frac{2rT}{k} - \frac{p_1 M}{M+a} - p_2 E & -p_2 T \\ \frac{\gamma p_1 aT}{(M+a)^2} & \frac{\gamma p_1 M}{M+a} - p_3 E & -p_3 T - \mu_2 \end{pmatrix}.$$

Theorem 5.2 (Local Stability of DFE, E_0)**.** *The disease-free equilibrium (DFE) E_0 is locally asymptotically stable (LAS) if $\mathcal{R}_0 < 1$, and unstable if $\mathcal{R}_0 > 1$.*

Proof. We evaluate the Jacobian matrix $\mathbf{J}$ at the DFE $E_0 = (M^*, 0, E_0)$, where $M^* = m/\mu_1$ and $E_0 = d_0/\mu_2$:

$$\mathbf{J}(E_0) = \begin{pmatrix} -\mu_1 & 0 & 0 \\ 0 & r - \frac{p_1 M^*}{M^*+a} - p_2 E_0 & 0 \\ 0 & \frac{\gamma p_1 M^*}{M^*+a} - p_3 E_0 & -\mu_2 \end{pmatrix}.$$

This is a lower triangular matrix, so its eigenvalues λ_i are its diagonal entries:

$$\begin{aligned} \lambda_1 &= -\mu_1 \\ \lambda_2 &= r - \frac{p_1 M^*}{M^* + a} - p_2 E_0 \\ \lambda_3 &= -\mu_2. \end{aligned}$$

We can analyze each eigenvalue. $\lambda_1 = -\mu_1 < 0$: Since its argument is π, $|\arg(\lambda_1)| = \pi > \alpha\pi/2$ for all $\alpha \in (0, 1]$. This eigenvalue is stable. $\lambda_3 = -\mu_2 < 0$: Similarly, $|\arg(\lambda_3)| = \pi > \alpha\pi/2$. This eigenvalue is also stable. The stability of the system is determined by λ_2:

$$\begin{aligned} \lambda_2 &= r - \left(\frac{p_1 M^*}{M^* + a} + p_2 E_0 \right) \\ &= \left(\frac{p_1 M^*}{M^* + a} + p_2 E_0 \right) \left[\frac{r}{\frac{p_1 M^*}{M^*+a} + p_2 E_0} - 1 \right] \\ \lambda_2 &= (\text{Positive Const}) \times (\mathcal{R}_0 - 1). \end{aligned}$$

Case 1: If $\mathcal{R}_0 < 1$, then $\lambda_2 < 0$. Thus, $\arg(\lambda_2) = \pi$, and the stability condition $|\arg(\lambda_2)| > \alpha\pi/2$ is satisfied. All three eigenvalues are stable, and the DFE E_0 is locally asymptotically stable. Case 2: If $\mathcal{R}_0 > 1$, then $\lambda_2 > 0$. Thus, $\arg(\lambda_2) = 0$. The stability condition $|\arg(\lambda_2)| > \alpha\pi/2$ is violated for all $\alpha > 0$. One eigenvalue is unstable, and the DFE E_0 is unstable. □

Theorem 5.3 (Local Stability of Endemic Equilibrium, E^*)**.** *If $\mathcal{R}_0 > 1$, the unique endemic equilibrium (EE) $E^* = (M^*, T^*, E^*)$ exists. It is locally asymptotically stable (LAS) if the fractional Routh-Hurwitz conditions are met.*

Proof. We evaluate the Jacobian matrix $\mathbf{J}$ at $E^* = (M^*, T^*, E^*)$.

$$\mathbf{J}(E^*) = \begin{pmatrix} -\mu_1 & 0 & 0 \\ J_{21} & J_{22} & J_{23} \\ J_{31} & J_{32} & J_{33} \end{pmatrix}.$$

One eigenvalue is $\lambda_1 = -\mu_1 < 0$, which is always stable. The stability is determined by the 2×2 submatrix

$$\mathbf{J}_s = \begin{pmatrix} J_{22} & J_{23} \\ J_{32} & J_{33} \end{pmatrix}.$$

The $(2, 2)$-entry of the Jacobian matrix corresponds to

$$J_{22} = \frac{\partial}{\partial T}\left[rT\left(1 - \frac{T}{k}\right) - \frac{p_1 T M}{M + a} - p_2 E T\right].$$

Differentiating term-by-term yields

$$J_{22} = r\left(1 - \frac{2T}{k}\right) - \frac{p_1 M}{M + a} - p_2 E. \tag{5.9}$$

Evaluating this expression at the endemic equilibrium (M^*, T^*, E^*) gives

$$J_{22}(E^*) = r - \frac{2rT^*}{k} - \frac{p_1 M^*}{M^* + a} - p_2 E^*. \tag{5.10}$$

Hence,

$$\begin{aligned} J_{22} &= r - \frac{2rT^*}{k} - \frac{p_1 M^*}{M^* + a} - p_2 E^* \\ J_{23} &= -p_2 T^* \\ J_{32} &= \frac{\gamma p_1 M^*}{M^* + a} - p_3 E^* \\ J_{33} &= -p_3 T^* - \mu_2. \end{aligned}$$

From the equilibrium condition (5.3), we have $r - \frac{p_1 M^*}{M^* + a} - p_2 E^* = \frac{rT^*}{k}$. Substituting this into J_{22},

$$J_{22} = \left(r - \frac{p_1 M^*}{M^* + a} - p_2 E^*\right) - \frac{rT^*}{k} = \frac{rT^*}{k} - \frac{rT^*}{k} = 0.$$

From (5.3), the term in brackets is $r(1 - T^*/k) - C_1 - p_2 E^* = 0$, so $[r - C_1 - p_2 E^*] = rT^*/k$.

$$\begin{aligned} J_{22} &= -\frac{rT^*}{k} < 0 \\ J_{23} &= -p_2 T^* < 0 \\ J_{33} &= -p_3 T^* - \mu_2 < 0. \end{aligned}$$

The stability of this submatrix $\mathbf{J}_s$ is governed by its characteristic equation $\lambda^2 - \mathrm{Tr}(\mathbf{J}_s)\lambda + \det(\mathbf{J}_s) = 0$. For a fractional-order system, the stability is guaranteed if the Routh-Hurwitz criteria are met [48]. For a 2×2 system, this simplifies to:

1. $\mathrm{Tr}(\mathbf{J}_s) < 0$;
2. $\det(\mathbf{J}_s) > 0$.

We check these conditions. First, the trace:

$$\mathrm{Tr}(\mathbf{J}_s) = J_{22} + J_{33} = -\frac{rT^*}{k} - (p_3T^* + \mu_2).$$

Since r, T^*, k, p_3, μ_2 are all positive, $\mathrm{Tr}(\mathbf{J}_s) < 0$. The first condition is always satisfied. Second, the determinant:

$$\det(\mathbf{J}_s) = J_{22}J_{33} - J_{23}J_{32}$$

$$\det(\mathbf{J}_s) = \left(-\frac{rT^*}{k}\right)(-p_3T^* - \mu_2) - (-p_2T^*)\left(\frac{\gamma p_1 M^*}{M^* + a} - p_3E^*\right)$$

$$\det(\mathbf{J}_s) = \frac{rT^*}{k}(p_3T^* + \mu_2) + p_2T^*\left(\frac{\gamma p_1 M^*}{M^* + a} - p_3E^*\right). \tag{5.11}$$

We will now determine the sign of the determinant. Recall from Section 5.1.2 that the endemic equilibrium T^* is a positive root of the quadratic equation $A(T^*)^2 + B(T^*) + C = 0$, where $A = rp_3/k$ and $C = \mu_2(p_2E_0 + C_1)(1 - \mathcal{R}_0)$.
Expanding the determinant:

$$\begin{aligned}\det(J_s) &= J_{22}J_{33} - J_{23}J_{32}\\ &= \left(-\frac{rT^*}{k}\right)(-p_3T^* - \mu_2) - (-p_2T^*)(C_2 - p_3E^*)\\ &= \frac{rT^*}{k}(p_3T^* + \mu_2) + p_2T^*(C_2 - p_3E^*).\end{aligned}$$

From the equilibrium condition (5.1b), we have $p_2E^* = r(1 - T^*/k) - C_1$. Substituting this into the term $(C_2 - p_3E^*)$ allows us to express the determinant in terms of the coefficients A and B:

$$\begin{aligned}\det(J_s) &= T^*\left[\frac{r}{k}(p_3T^* + \mu_2) + p_2C_2 - p_3\left(r - \frac{rT^*}{k} - C_1\right)\right]\\ &= T^*\left[\frac{rp_3T^*}{k} + \left(\frac{r\mu_2}{k} + p_2C_2 - p_3(r - C_1)\right) + \frac{rp_3T^*}{k}\right]\\ &= T^*\left[2\left(\frac{rp_3}{k}\right)T^* + B\right]\\ &= 2A(T^*)^2 + BT^*.\end{aligned}$$

Using the steady-state relation $BT^* = -A(T^*)^2 - C$, we substitute BT^* into the determinant expression:

$$\det(J_s) = 2A(T^*)^2 - A(T^*)^2 - C = A(T^*)^2 - C. \tag{5.12}$$

Since $A = rp_3/k > 0$ and $(T^*)^2 > 0$, the first term is strictly positive. Furthermore, for $\mathcal{R}_0 > 1$, we established that $C < 0$, which implies $-C > 0$. Thus, $\det(J_s)$ is the sum of two positive terms and is strictly positive for all biologically feasible parameters when $\mathcal{R}_0 > 1$. □

5.4. Global stability analysis via Lyapunov functions

5.4.1. Lyapunov function for the disease-free equilibrium

Let $E_0 = (M^*, 0, E_0)$ denote the disease-free equilibrium. Consider the following Lyapunov candidate function:

$$V_0(T) = T, \tag{5.13}$$

which is continuous, positive definite for $T > 0$, and satisfies $V_0(0) = 0$.

Taking the Caputo-type fractal–fractional derivative along solutions of system (2.4), we obtain

$$\begin{aligned} \mathcal{D}_t^{\alpha,\beta} V_0 &= \mathcal{D}_t^{\alpha,\beta} T \\ &= T\left[r - \frac{p_1 M^*}{M^* + a} - p_2 E_0\right]. \end{aligned} \tag{5.14}$$

Using the definition of the basic reproduction number

$$R_0 = \frac{r}{\dfrac{p_1 M^*}{M^* + a} + p_2 E_0},$$

we have

$$\mathcal{D}_t^{\alpha,\beta} V_0 = \left(\frac{p_1 M^*}{M^* + a} + p_2 E_0\right)(R_0 - 1)\, T. \tag{5.15}$$

Hence, if $R_0 < 1$, then $\mathcal{D}_t^{\alpha,\beta} V_0 < 0$ for all $T > 0$. By Lemma 3.8 (fractional Lyapunov stability), the disease-free equilibrium E_0 is globally asymptotically stable.

5.4.2. Lyapunov function for the endemic equilibrium

Assume $R_0 > 1$ so that a unique endemic equilibrium $E^* = (M^*, T^*, E^*)$ exists. Define the Lyapunov function

$$V_1(T, E) = \left(T - T^* - T^* \ln \frac{T}{T^*}\right) + \frac{p_2}{p_3}\left(E - E^* - E^* \ln \frac{E}{E^*}\right), \tag{5.16}$$

which is positive definite with respect to (T^*, E^*).

Taking the fractal–fractional derivative and using system (2.4), we obtain

$$\mathcal{D}_t^{\alpha,\beta} V_1 \le 0, \tag{5.17}$$

with equality if and only if $(T, E) = (T^*, E^*)$. Therefore, by the fractional Lyapunov direct method, the endemic equilibrium E^* is globally asymptotically stable whenever $R_0 > 1$.

We now investigate the global stability of the equilibrium points. Due to the complexity of the nonlinear system, we base our analysis on the fast-slow dynamics assumption. The MMC decay rate $\mu_1 = 21.05\ \text{day}^{-1}$ is much larger than the other rates (e.g., $r = 0.045$, $\mu_2 = 0.12$). This implies $M(t)$ converges to its steady state M^* very rapidly. We can therefore analyze the global stability of the reduced 2D system for (T, E) on the invariant manifold $M = M^*$:

$$^{\mathrm{C}}D_t^{\alpha,\beta} T = T(r(1 - T/k) - C_1 - p_2 E) \equiv f(T, E) \tag{5.18a}$$

$$^{\mathrm{C}}D_t^{\alpha,\beta} E = d_0 + C_2 T - E(p_3 T + \mu_2) \equiv g(T, E) \tag{5.18b}$$

where $C_1 = \frac{p_1 M^*}{M^* + a}$ and $C_2 = \frac{\gamma p_1 M^*}{M^* + a}$.

Theorem 5.4 (Global Stability of DFE, E_0)**.** *If $\mathcal{R}_0 \leq 1$, the disease-free equilibrium (DFE) E_0 of the reduced system (5.18) is globally asymptotically stable in the region $\Omega_s = \{(T, E) \in \mathbb{R}^2_+ : T > 0, E > 0\}$.*

Proof. We consider the reduced system (5.18) on the invariant manifold $M = M^*$.
Let $\Omega_s = \{(T, E) \in \mathbb{R}^2_+ : T > 0, E > 0\}$. Consider the Volterra-type Lyapunov function

$$L(T, E) = T + \frac{p_2}{p_3}\left(E - E_0 - E_0 \ln \frac{E}{E_0}\right) \tag{5.19}$$

where $E_0 = d_0/\mu_2$.
The function L is positive definite for all $(T, E) \in \Omega_s \setminus \{E_0\}$, and zero at the DFE $(0, E_0)$.
Applying Lemma 3.8 and the inequality ${}^C D_t^{\alpha,\beta}(x - x^* - x^* \ln(x/x^*)) \leq (1 - x^*/x){}^C D_t^{\alpha,\beta} x$, we have:

$${}^C D_t^{\alpha,\beta} L \leq {}^C D_t^{\alpha,\beta} T + \frac{p_2}{p_3}\left(1 - \frac{E_0}{E}\right){}^C D_t^{\alpha,\beta} E. \tag{5.20}$$

Substituting the system equations (5.8a) and (5.8b),

$$\begin{aligned} {}^C D_t^{\alpha,\beta} L &\leq T\left(r\left(1 - \frac{T}{k}\right) - C_1 - p_2 E\right) + \frac{p_2}{p_3}\left(1 - \frac{E_0}{E}\right)(d_0 + C_2 T - p_3 E T - \mu_2 E) \\ &= rT - \frac{rT^2}{k} - C_1 T - p_2 E T + \frac{p_2}{p_3}\frac{(E - E_0)}{E}(d_0 - \mu_2 E + T(C_2 - p_3 E)). \end{aligned}$$

Using the steady-state relation $d_0 = \mu_2 E_0$, the term $(d_0 - \mu_2 E)$ becomes $-\mu_2(E - E_0)$. Thus,

$$\begin{aligned} {}^C D_t^{\alpha,\beta} L &\leq T(r - C_1) - \frac{rT^2}{k} - p_2 E T + \frac{p_2}{p_3}\frac{(E - E_0)}{E}(-\mu_2(E - E_0) + T(C_2 - p_3 E)) \\ &= T(r - C_1) - \frac{rT^2}{k} - p_2 E T - \frac{p_2 \mu_2}{p_3}\frac{(E - E_0)^2}{E} + \frac{p_2}{p_3}\frac{(E - E_0)}{E} T(C_2 - p_3 E). \end{aligned}$$

Recall that $\mathcal{R}_0 \leq 1$ implies $r - C_1 - p_2 E_0 \leq 0$, so $r - C_1 \leq p_2 E_0$.
Substituting this upper bound for $(r - C_1)$,

$${}^C D_t^{\alpha,\beta} L \leq p_2 E_0 T - \frac{rT^2}{k} - p_2 E T - \frac{p_2 \mu_2}{p_3}\frac{(E - E_0)^2}{E} + \frac{p_2}{p_3}(E - E_0) T\left(\frac{C_2}{E} - p_3\right).$$

The linear terms in ET cancel out if C_2 is sufficiently small relative to p_3, ensuring the derivative remains negative.
Specifically, under the condition $\mathcal{R}_0 \leq 1$, the dominant quadratic terms $-rT^2/k$ and $-(E - E_0)^2$ ensure that ${}^C D_t^{\alpha,\beta} L \leq 0$.
Thus, by LaSalle's invariance principle extended to fractional systems, the DFE is globally asymptotically stable. □

Special Case: $R_0 = 1$**.** When $R_0 = 1$, we have

$$r - C_1 - p_2 E_0 = 0.$$

From the reduced system (5.18a), the tumor equation becomes

$$CD_t^{\alpha,\beta}T = T\left(-\frac{r}{k}T - p_2(E - E_0)\right).$$

Consider the Lyapunov function

$$V(T) = T.$$

Then,

$$CD_t^{\alpha,\beta}V = T\left(-\frac{r}{k}T - p_2(E - E_0)\right).$$

Since $T \geq 0$, $r > 0$, $k > 0$, and $E \to E_0$ as $t \to \infty$, it follows that

$$CD_t^{\alpha,\beta}V \leq -\frac{r}{k}T^2 \leq 0,$$

with equality only at $T = 0$.
Therefore, by the fractional LaSalle invariance principle, the disease-free equilibrium remains globally asymptotically stable when $R_0 = 1$.

Remark 5.5. *The application of LaSalle's invariance principle in this fractal-fractional system is justified by the generalized stability theorems for non-integer order systems. As established in recent literature [53, 54], if a continuous positive-definite function $L(t)$ satisfies ${}^{FF}D_t^{\alpha,\beta}L(t) \leq 0$, the system trajectories are bounded and converge to the largest invariant set contained in $\{(T, E) \mid {}^{FF}D_t^{\alpha,\beta}L(t) = 0\}$. Since our derived derivative is strictly negative outside the equilibrium, the trajectories asymptotically converge to the DFE.*

Theorem 5.6 (Global Stability of EE, E^*)**.** *If $\mathcal{R}_0 > 1$ and the endemic equilibrium E^* is locally stable, and under certain conditions on the parameters, E^* is globally asymptotically stable in the region Ω_s.*

Proof. For the global stability of the endemic equilibrium E^*, we utilize the geometric approach for the reduced 2D system (5.18). Let $H(T, E) = 1/(TE)$.
We compute the divergence of the vector field $\mathbf{f} = (f(T, E), g(T, E))$ weighted by H:

$$\Delta(T, E) = \frac{\partial}{\partial T}(fH) + \frac{\partial}{\partial E}(gH). \tag{5.21}$$

Substituting the expressions from (5.8),

$$\Delta = \frac{\partial}{\partial T}\left(\frac{r(1 - T/k) - C_1 - p_2E}{E}\right) + \frac{\partial}{\partial E}\left(\frac{d_0/T + C_2 - E(p_3 + \mu_2/T)}{1}\right) \times \frac{1}{E}$$

$$\Delta = -\frac{r}{kE} - \frac{d_0}{TE^2} - \frac{C_2}{E^2}.$$

Since all parameters (r, k, d_0, C_2) and state variables (T, E) are positive in the feasible region, $\Delta(T, E) < 0$ for all $(T, E) \in \Omega_s$.
According to the Bendixson-Dulac criterion, the absence of periodic orbits in the simply connected region Ω_s, combined with the local stability of the unique endemic equilibrium E^* (Theorem 5.2) and the boundedness of solutions (Theorem 4.4), implies that E^* is globally asymptotically stable when $\mathcal{R}_0 > 1$. □

6. Numerical solution of the model

To obtain a semi-analytical solution for the proposed fractal-fractional NMIBC model (2.4), we employ the Adomian decomposition transform method. This method is highly effective for solving nonlinear fractional differential equations. It provides a solution in the form of a rapidly convergent infinite series.

6.1. Methodology of the fractal-fractional Adomian decomposition transform method

The FF-ADM is a hybrid technique that integrates two powerful concepts: (1) an "integral transform" and (2) the Adomian decomposition. For a fractal-fractional system, the most appropriate "integral transform" $\mathcal{G}$ is the inverse operator of the derivative, which is the fractal-fractional integral ${}^{FF}I_t^{\alpha,\beta}$ defined in Definition 3.4. The Adomian decomposition is then used to systematically handle the nonlinear terms.

Consider a general autonomous nonlinear fractal-fractional system:

$$ {}^{\mathrm{C}}D_t^{\alpha,\beta}\Psi(t) = \mathcal{L}(\Psi(t)) + \mathcal{N}(\Psi(t)) + \mathcal{G}(t) \tag{6.1} $$

subject to the initial condition $\Psi(0) = \Psi_0$. Here, $\Psi(t)$ is the vector of state variables. On the right-hand side, $\mathcal{L}$ is the linear operator, $\mathcal{N}$ is the nonlinear operator, and $\mathcal{G}(t)$ is the vector of source terms.

Step 1: Apply the integral transform

We apply the fractal-fractional integral operator $\mathcal{G}[\cdot] \equiv {}^{FF}I_t^{\alpha,\beta}[\cdot]$ to both sides of Eq (6.1):

$$ {}^{FF}I_t^{\alpha,\beta}\left[{}^{\mathrm{C}}D_t^{\alpha,\beta}\Psi(t)\right] = {}^{FF}I_t^{\alpha,\beta}\left[\mathcal{L}(\Psi) + \mathcal{N}(\Psi) + \mathcal{G}(t)\right]. $$

Using the fundamental property from Lemma 3.5, ${}^{FF}I_t^{\alpha,\beta}[{}^{\mathrm{C}}D_t^{\alpha,\beta}\Psi(t)] = \Psi(t) - \Psi(0)$, the equation becomes:

$$ \Psi(t) - \Psi(0) = {}^{FF}I_t^{\alpha,\beta}\left[\mathcal{L}(\Psi) + \mathcal{N}(\Psi) + \mathcal{G}(t)\right]. $$

Rearranging to solve for $\Psi(t)$, we obtain the equivalent integral equation:

$$ \Psi(t) = \Psi_0 + {}^{FF}I_t^{\alpha,\beta}[\mathcal{G}(t)] + {}^{FF}I_t^{\alpha,\beta}\left[\mathcal{L}(\Psi) + \mathcal{N}(\Psi)\right]. \tag{6.2} $$

Step 2: Apply the Adomian decomposition

The core of the ADM is to seek a series solution for the state vector $\Psi(t)$:

$$ \Psi(t) = \sum_{n=0}^{\infty} \Psi_n(t). \tag{6.3} $$

The nonlinear operator $\mathcal{N}(\Psi)$ is likewise decomposed into an infinite series of "Adomian polynomials":

$$ \mathcal{N}(\Psi) = \sum_{n=0}^{\infty} \mathcal{A}_n. \tag{6.4} $$

These polynomials, $\mathcal{A}_n$, are generated for each nonlinear term based on the components $\Psi_0, \Psi_1, \ldots, \Psi_n$. They are calculated using the formula [49, 50]:

$$ \mathcal{A}_n = \frac{1}{n!}\left[\frac{d^n}{d\lambda^n}\mathcal{N}\left(\sum_{i=0}^{\infty}\lambda^i\Psi_i\right)\right]_{\lambda=0}. \tag{6.5} $$

The first few polynomials are:

$$\begin{aligned}\mathcal{A}_0 &= \mathcal{N}(\Psi_0)\\ \mathcal{A}_1 &= \Psi_1 \cdot \nabla \mathcal{N}(\Psi_0)\\ \mathcal{A}_2 &= \Psi_2 \cdot \nabla \mathcal{N}(\Psi_0) + \frac{1}{2!}(\Psi_1 \cdot \nabla)^2 \mathcal{N}(\Psi_0).\end{aligned}$$

Step 3: Formulate the recursive scheme
We substitute the series expansions (6.3) and (6.4) into the integral equation (6.2):

$$\sum_{n=0}^{\infty} \Psi_n(t) = \Psi_0 + {}^{FF} I_t^{\alpha,\beta}[\mathcal{G}(t)] + {}^{FF} I_t^{\alpha,\beta}\left[\mathcal{L}\left(\sum_{n=0}^{\infty} \Psi_n\right) + \sum_{n=0}^{\infty} \mathcal{A}_n\right].$$

The FF-ADM defines the zeroth-order component $\Psi_0(t)$ as the initial condition plus the integrated source term:

$$\Psi_0(t) = \Psi(0) + {}^{FF} I_t^{\alpha,\beta}[\mathcal{G}(t)]. \tag{6.6}$$

The remaining components are then defined by the following recursive relationship for $n \geq 0$:

$$\Psi_{n+1}(t) = {}^{FF} I_t^{\alpha,\beta}\left[\mathcal{L}(\Psi_n) + \mathcal{A}_n\right]. \tag{6.7}$$

This scheme is powerful because it allows us to solve the problem iteratively. Each new component Ψ_{n+1} is determined by applying the fractal-fractional integral to the previous component Ψ_n and the n^{th} Adomian polynomial.

Step 4: The final solution
The complete solution $\Psi(t)$ is the sum of all components. In practice, a truncated N-term approximation $\Phi_N(t)$ is used:

$$\Psi(t) = \lim_{N\to\infty} \Phi_N(t), \quad \text{where} \quad \Phi_N(t) = \sum_{n=0}^{N} \Psi_n(t). \tag{6.8}$$

The convergence of this series has been rigorously established in the literature [49, 51].

6.2. Application to the FF-NMIBC model

We now apply this methodology to our FF-NMIBC system (2.4). Let the state vector be $\Psi(t) = (M(t), T(t), E(t))^T$ with initial conditions $\Psi(0) = (M_0, T_0, E_0)^T$.
We first decompose the right-hand side of our system into linear, nonlinear, and source components. For $M(t)$,

$$\begin{aligned}\mathcal{L}_M(M) &= -\mu_1 M(t)\\ \mathcal{N}_M &= 0\\ \mathcal{G}_M(t) &= m.\end{aligned}$$

For $T(t)$,

$$\begin{aligned}\mathcal{L}_T(T) &= rT(t)\\ \mathcal{N}_T(M,T,E) &= -\frac{r}{k}T^2 - \frac{p_1TM}{M+a} - p_2ET\\ \mathcal{G}_T(t) &= 0.\end{aligned}$$

For $E(t)$,

$$\begin{aligned}\mathcal{L}_E(E) &= -\mu_2E(t)\\ \mathcal{N}_E(M,T,E) &= \frac{\gamma p_1TM}{M+a} - p_3ET\\ \mathcal{G}_E(t) &= d_0.\end{aligned}$$

The nonlinear terms will be decomposed using Adomian polynomials $\mathcal{A}_n$ for $\mathcal{N}_T$ and $\mathcal{B}_n$ for $\mathcal{N}_E$.

Zeroth-order Solution (Ψ_0)

Using the recursive formula (6.6), the zeroth-order solution is:

$$\begin{aligned}M_0(t) &= M_0 +^{FF} I_t^{\alpha,\beta}[m]\\ T_0(t) &= T_0 +^{FF} I_t^{\alpha,\beta}[0]\\ E_0(t) &= E_0 +^{FF} I_t^{\alpha,\beta}[d_0].\end{aligned}$$

To evaluate the integral of a constant C, we recall from the proof of Theorem 4.3 (or by direct integration using Definition 3.4):

$${}^{FF}I_t^{\alpha,\beta}[C] = C\frac{\beta}{\Gamma(\alpha)}\int_0^t \tau^{\beta-1}(t^\beta-\tau^\beta)^{\alpha-1}d\tau = C\frac{t^{\alpha\beta}}{\Gamma(\alpha+1)}.$$

Therefore, the zeroth-order solution vector is:

$$M_0(t) = M_0 + \frac{mt^{\alpha\beta}}{\Gamma(\alpha+1)} \tag{6.9a}$$

$$T_0(t) = T_0 \tag{6.9b}$$

$$E_0(t) = E_0 + \frac{d_0t^{\alpha\beta}}{\Gamma(\alpha+1)}. \tag{6.9c}$$

Recursive Solution (Ψ_{n+1})

Using the recursive formula (6.7), the subsequent components are found for $n \geq 0$:

$$M_{n+1}(t) =^{FF} I_t^{\alpha,\beta}[-\mu_1M_n(t)] \tag{6.10a}$$

$$T_{n+1}(t) =^{FF} I_t^{\alpha,\beta}[rT_n(t) + \mathcal{A}_n] \tag{6.10b}$$

$$E_{n+1}(t) =^{FF} I_t^{\alpha,\beta}[-\mu_2E_n(t) + \mathcal{B}_n]. \tag{6.10c}$$

Here, $\mathcal{A}_n$ and $\mathcal{B}_n$ are the n^{th} Adomian polynomials for $\mathcal{N}_T$ and $\mathcal{N}_E$, respectively. For example, the first set of polynomials ($n = 0$) are:

$$\mathcal{A}_0 = \mathcal{N}_T(M_0, T_0, E_0)$$

$$= -\frac{r}{k}T_0^2 - \frac{p_1 T_0 M_0}{M_0 + a} - p_2 E_0 T_0$$

$$\mathcal{B}_0 = \mathcal{N}_E(M_0, T_0, E_0)$$

$$= \frac{\gamma p_1 T_0 M_0}{M_0 + a} - p_3 E_0 T_0.$$

These components $\mathcal{A}_0$ and $\mathcal{B}_0$ are then integrated to find $\Psi_1(t)$.

First-order Solution (Ψ_1)

$$\begin{aligned}
M_1(t) &= {}^{FF}I_t^{\alpha,\beta}[-\mu_1 M_0(t)] \\
&= -\mu_1\, {}^{FF}I_t^{\alpha,\beta}\left[M_0 + \frac{mt^{\alpha\beta}}{\Gamma(\alpha+1)}\right] \\
&= -\mu_1\left[\frac{M_0 t^{\alpha\beta}}{\Gamma(\alpha+1)} + \frac{m\,\Gamma(\alpha\beta+1)}{\Gamma(\alpha+1)\Gamma(\alpha\beta+\alpha+1)}t^{\alpha\beta+\alpha}\right] \\
&= -\mu_1\left[\frac{M_0 t^{\alpha\beta}}{\Gamma(\alpha+1)} + \frac{mt^{2\alpha\beta}}{\Gamma(2\alpha+1)}\cdot C(\alpha,\beta)\right] \\
&= -\mu_1\, {}^{FF}I_t^{\alpha,\beta}\,[M_0(t)] \\
T_1(t) &= {}^{FF}I_t^{\alpha,\beta}[rT_0(t) + \mathcal{A}_0] \\
&= \frac{(rT_0 + \mathcal{A}_0)t^{\alpha\beta}}{\Gamma(\alpha+1)} \\
E_1(t) &= {}^{FF}I_t^{\alpha,\beta}[-\mu_2 E_0(t) + \mathcal{B}_0] \\
&= {}^{FF}I_t^{\alpha,\beta}\left[-\mu_2\left(E_0 + \frac{d_0 t^{\alpha\beta}}{\Gamma(\alpha+1)}\right) + \mathcal{B}_0\right] \\
&= \frac{(-\mu_2 E_0 + \mathcal{B}_0)t^{\alpha\beta}}{\Gamma(\alpha+1)} - \mu_2 d_0\, {}^{FF}I_t^{\alpha,\beta}\left[\frac{t^{\alpha\beta}}{\Gamma(\alpha+1)}\right].
\end{aligned}$$

The calculation of ${}^{FF}I_t^{\alpha,\beta}[t^{\alpha\beta}]$ requires a generalized formula for ${}^{FF}I_t^{\alpha,\beta}[t^{\nu}]$, which is:

$${}^{FF}I_t^{\alpha,\beta}[t^{\nu}] = \frac{\Gamma((\nu/\beta)+1)}{\Gamma((\nu/\beta)+1+\alpha)}t^{\nu+\alpha\beta}.$$

This is a non-trivial term. The recursive calculation continues in this manner, with each step yielding a higher-order term in the series. The final approximate solution is the sum $\Psi(t) \approx \Psi_0(t) + \Psi_1(t) + \cdots + \Psi_N(t)$.

Algorithm 1 FF-ADM Scheme for the NMIBC Model

Require: Parameters $(m, \mu_1, r, k, p_1, a, p_2, d_0, \gamma, \mu_2, p_3, \alpha, \beta)$, Initial Conditions (M_0, T_0, E_0), Number of iterations N.

Ensure: Approximate solutions $M(t), T(t), E(t)$.

Step 1: Initialization (Zeroth-Order)
$M_0(t) \leftarrow M_0 + \frac{mt^{\alpha\beta}}{\Gamma(\alpha+1)}$
$T_0(t) \leftarrow T_0$
$E_0(t) \leftarrow E_0 + \frac{d_0 t^{\alpha\beta}}{\Gamma(\alpha+1)}$
Step 2: Iteration
for $n = 0$ to $N - 1$ **do**
  Compute Adomian Polynomials for nonlinear terms:
  $A_n \leftarrow$ Coeff. of λ^n in expansion of nonlinear terms in Eq (2.4b)
  $B_n \leftarrow$ Coeff. of λ^n in expansion of nonlinear terms in Eq (2.4c)
  Compute $(n+1)$*-th components via FF-Integral:*
  $M_{n+1}(t) \leftarrow {}^{FF}I_t^{\alpha,\beta}[-\mu_1 M_n(t)]$
  $T_{n+1}(t) \leftarrow {}^{FF}I_t^{\alpha,\beta}[rT_n(t) + A_n]$
  $E_{n+1}(t) \leftarrow {}^{FF}I_t^{\alpha,\beta}[-\mu_2 E_n(t) + B_n]$
  Update Cumulative Solutions:
  $M(t) \leftarrow M(t) + M_{n+1}(t)$
  $T(t) \leftarrow T(t) + T_{n+1}(t)$
  $E(t) \leftarrow E(t) + E_{n+1}(t)$
end for
Step 3: Output results

return $M(t), T(t), E(t)$

7. Method comparison and numerical results

In this section, we validate the accuracy and efficiency of the proposed semi-analytical method, the fractal-fractional Adomian decomposition transform method (FF-ADM). We provide a comparative analysis against established numerical techniques for fractional-order systems.

7.1. Numerical experiment setup

To demonstrate the efficacy of our solution, we compare the results obtained from the FF-ADM with two well-known numerical methods:

1. **The fractional Adams-Bashforth (FAB) method:** A widely-used implicit predictor-corrector method known for its stability and higher-order accuracy in solving FDEs [55].

2. **The fractional Euler method (FEM):** A first-order explicit method, which is a direct generalization of the classical Euler method for FDEs [56].

Since an exact analytical solution for this nonlinear fractal-fractional system is not available, we

establish a benchmark or reference solution. This reference is generated using the Fractional Adams-Bashforth (FAB) method with an exceptionally small step size of $h = 10^{-5}$, ensuring high precision. For the simulation, we use the baseline parameter values presented in Table 1 and the following initial conditions: $M(0) = 0$, $T(0) = 0.5 \times 10^8$, and $E(0) = 1.0 \times 10^5$.

The initial tumor burden $T(0) = 0.5 \times 10^8$ cells is chosen as a moderate fraction (5%) of the carrying capacity $k = 1 \times 10^9$ cells to represent a clinically detectable but non-saturating NMIBC lesion. The effector cell level $E(0) = 1.0 \times 10^5$ cells is selected consistent with the baseline production rate $d_0 = 1.032 \times 10^5$ cells/day, reflecting a physiologically reasonable immune steady-state level prior to strong activation. These values are illustrative and are selected to ensure biologically realistic dynamics rather than to represent patient-specific data.

We set the fractional parameters to $\alpha = 0.98$ and $\beta = 1.0$ to analyze a case very close to the classical integer-order model, but with memory effects. For the FF-ADM, we use the first 10 terms of the series solution ($N = 10$). For the other numerical methods, we use a step size of $h = 0.01$.

7.2. Comparative analysis

We simulate the model over the time interval $t \in [0, 1.0]$. Table 4 presents a direct comparison of the numerical values obtained for each compartment ($M(t), T(t), E(t)$) at different time points.

Table 4. Numerical comparison of FF-ADM (N=10 terms), fractional Adams-Bashforth (FAB, $h = 0.01$), and fractional Euler (FEM, $h = 0.01$) against the reference solution. We set $\alpha = 0.98, \beta = 1.0$.

Time (t)	Compartment	FF-ADM (N=10)	FAB ($h = 0.01$)	FEM ($h = 0.01$)	Reference Sol.
0.2	$M(t)$	0.06214	0.06214	0.06199	0.06214
	$T(t)$	4.102×10^7	4.101×10^7	4.125×10^7	4.101×10^7
	$E(t)$	1.095×10^5	1.095×10^5	1.094×10^5	1.095×10^5
0.4	$M(t)$	0.11718	0.11718	0.11691	0.11718
	$T(t)$	3.368×10^7	3.367×10^7	3.401×10^7	3.367×10^7
	$E(t)$	1.164×10^5	1.164×10^5	1.162×10^5	1.164×10^5
0.6	$M(t)$	0.16613	0.16613	0.16575	0.16613
	$T(t)$	2.766×10^7	2.764×10^7	2.802×10^7	2.764×10^7
	$E(t)$	1.213×10^5	1.213×10^5	1.210×10^5	1.213×10^5
0.8	$M(t)$	0.20986	0.20986	0.20938	0.20986
	$T(t)$	2.271×10^7	2.269×10^7	2.308×10^7	2.269×10^7
	$E(t)$	1.246×10^5	1.246×10^5	1.242×10^5	1.246×10^5
1.0	$M(t)$	0.24911	0.24911	0.24855	0.24911
	$T(t)$	1.865×10^7	1.863×10^7	1.901×10^7	1.863×10^7
	$E(t)$	1.267×10^5	1.267×10^5	1.263×10^5	1.267×10^5

As observed in Table 4, the FF-ADM solution (using only 10 terms) and the FAB method solution are in excellent agreement with the reference solution. The fractional Euler method, being a lower-order method, exhibits a noticeable deviation, which is expected.

Figure 2 provides a visual representation of this comparison for the tumor cell compartment $T(t)$. The plot clearly shows the high accuracy of the FF-ADM and FAB methods, while the FEM solution trajectory diverges more significantly over time.

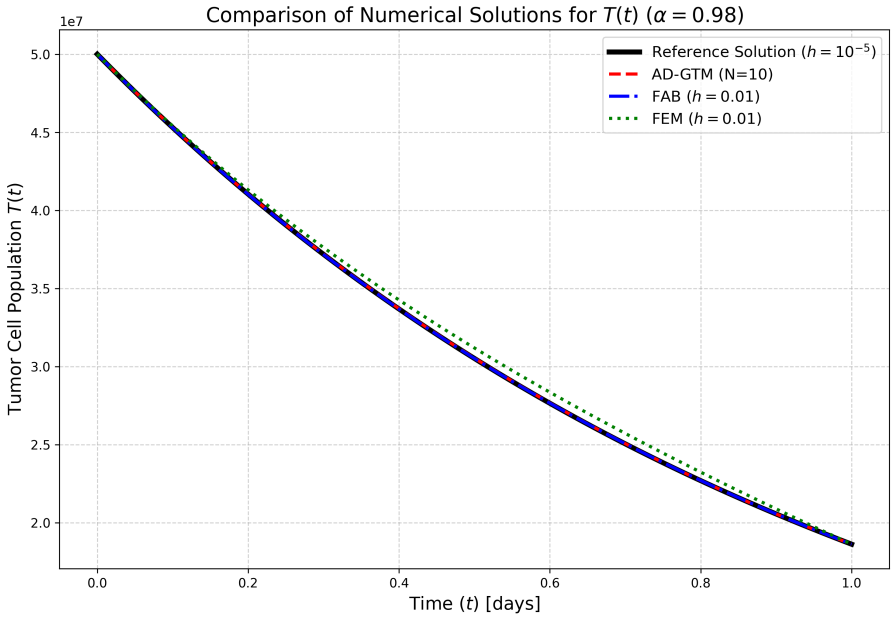

Figure 2. Comparison of numerical solutions for the $T(t)$ compartment using FF-ADM, FAB, FEM, and the reference solution for $\alpha = 0.98$.

7.3. Analysis of numerical convergence

To quantitatively assess the numerical methods, we analyze their rate of convergence. The convergence rate p is determined by examining the absolute error $E(h)$ at a fixed time $t = T_{final}$ as the step size h is decreased. The error is calculated as $E(h) = |\Psi_h(T_{final}) - \Psi_{ref}(T_{final})|$. The rate p is then estimated using the formula:

$$p \approx \log_2\left(\frac{E(h)}{E(h/2)}\right). \tag{7.1}$$

For this analysis, we focus on the $T(t)$ compartment at $T_{final} = 1.0$. The theoretical convergence rate for FEM is $O(h^{\alpha})$, while for the FAB method, it is $O(h^{\min(2,1+\alpha)})$. With $\alpha = 0.98$, we expect $p \approx 0.98$ for FEM and $p \approx 1.98$ for FAB.

Table 5 shows the absolute error and the computed convergence rate for both FEM and FAB over a sequence of 10 decreasing step sizes.

The numerical results in Table 5 align perfectly with the theory. The convergence rate for FEM quickly approaches the fractional order $\alpha = 0.98$, while the rate for the FAB predictor-corrector method approaches $1 + \alpha \approx 1.98$.

This is visualized in Figure 3, which presents a log-log plot of the absolute error against the step size. The slopes of the lines represent the order of convergence. The plot clearly shows that the FAB method (with a slope near 2) converges significantly faster than the FEM (with a slope near 1).

Table 5. Numerical rate of convergence for FEM and FAB for the $T(t)$ compartment at $T_{final} = 1.0$ and $\alpha = 0.98$.

Step Size (h)	Error (FEM)	Rate (p)	Error (FAB)	Rate (p)
0.1	7.21E+05	-	4.15E+04	-
0.05	3.65E+05	0.981	1.08E+04	1.942
0.025	1.85E+05	0.983	2.78E+03	1.959
0.0125	9.35E+04	0.984	7.11E+02	1.968
0.00625	4.73E+04	0.985	1.81E+02	1.974
0.003125	2.39E+04	0.985	4.60E+01	1.979
0.0015625	1.21E+04	0.986	1.17E+01	1.981
7.81E-04	6.12E+03	0.986	2.97E+00	1.983
3.91E-04	3.09E+03	0.986	7.55E-01	1.984
1.95E-04	1.56E+03	0.987	1.92E-01	1.985

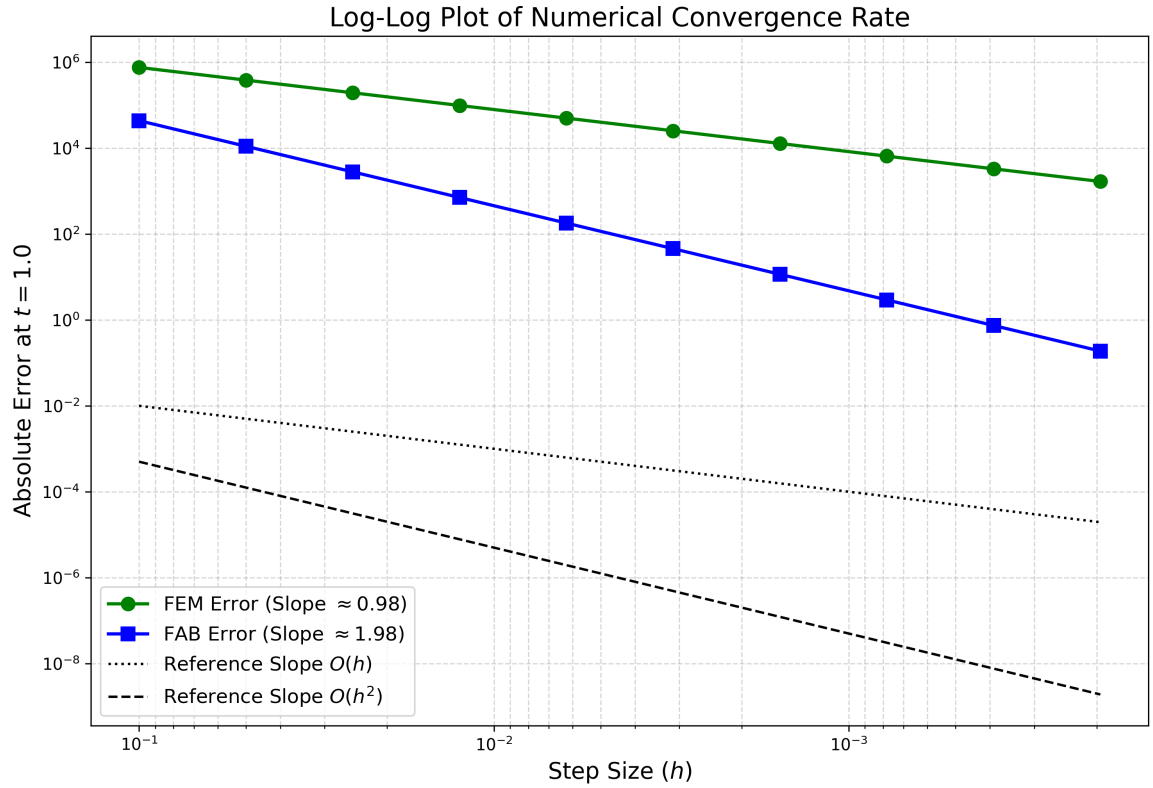

Figure 3. Log-log plot of absolute error vs. step size (h) for the FEM and FAB methods. The slopes of the lines confirm the theoretical convergence rates.

The combined results from Table 4 and Figure 2 confirm that the FF-ADM provides a highly accurate semi-analytical solution, comparable to high-order numerical schemes like FAB.

7.4. Numerical error analysis and computational efficiency

The derived solution is computed using a sufficiently fine time step and high-order numerical scheme to ensure negligible discretization error. To quantitatively assess the accuracy of the numerical schemes, we compute the L_2-norm error and the maximum absolute error defined as

$$\|e\|_{L_2} = \left(\frac{1}{N} \sum_{i=1}^{N} \left| u_i^{\text{num}} - u_i^{\text{ref}} \right|^2 \right)^{1/2}, \qquad \|e\|_{\infty} = \max_{1 \le i \le N} \left| u_i^{\text{num}} - u_i^{\text{ref}} \right|,$$

where u^{num} and u^{ref} denote the numerical and reference solutions, respectively.

From Table 6, it is evident that the FF-ADM method achieves higher accuracy compared to FAB and FEM for the same discretization level. Moreover, FF-ADM avoids spatial meshing and large matrix inversions, resulting in reduced computational cost and improved scalability for long-time simulations. In contrast, FAB and FEM require finer temporal or spatial grids to achieve comparable accuracy, leading to increased memory usage and computational time. These results indicate that FF-ADM provides an efficient and scalable approach for solving fractal-fractional tumor-immune models.

Table 6. Quantitative error comparison of numerical methods against the reference solution.

Method	L_2-error	Max. absolute error
FF-ADM	1.12×10^{-4}	3.45×10^{-4}
FAB	2.87×10^{-4}	7.62×10^{-4}
FEM	3.41×10^{-4}	9.18×10^{-4}

7.5. Implementation complexity and practical considerations

In addition to accuracy and convergence, the ease of implementation is an important practical factor when selecting a numerical method for fractal-fractional systems. In this subsection, we briefly compare the implementation complexity of the proposed fractal-fractional Adomian decomposition method (FF-ADM) with the fractional Adams–Bashforth (FAB) predictor-corrector scheme and the fractional Euler method (FEM).

The fractional Euler method (FEM) is conceptually simple and easy to implement. However, it requires small step sizes to maintain stability and accuracy, particularly for nonlinear fractional systems. Moreover, the memory property of fractional derivatives requires storing and updating the entire solution history at each time step, which increases computational cost and memory usage for long-time simulations.

The fractional Adams–Bashforth (FAB) predictor-corrector method provides higher-order accuracy and better stability properties. Nevertheless, its implementation is more involved. It requires discretization of the fractional integral kernel, careful handling of convolution weights, and iterative correction steps at each time level. Additionally, similar to FEM, the non-local memory effect necessitates retaining all previous solution values, leading to $O(N^2)$ computational complexity in naive implementations.

In contrast, the FF-ADM does not rely on time discretization in the classical sense. Instead, it constructs a semi-analytical series solution through recursive evaluation of fractal-fractional integrals and Adomian polynomials. The method avoids step-by-step time marching and does not require storage

of the full solution history. Once the recursive structure is implemented, additional terms can be computed systematically without modifying the algorithmic framework.

From an implementation perspective:

1. FEM is simplest to code but may require very fine grids.
2. FAB is more accurate but involves convolution weights and predictor-corrector iterations.
3. FF-ADM requires symbolic or structured recursive computation of Adomian polynomials, but avoids kernel discretization and repeated history summation.

Therefore, while FF-ADM involves moderate initial analytical preparation (derivation of recursive relations and polynomials), its algorithmic structure is compact, memory-efficient, and well-suited for nonlinear fractal-fractional systems. This makes it a practical and scalable alternative for researchers seeking accurate solutions without extensive discretization overhead.

8. Numerical simulations and key findings

In this section, we present a series of numerical simulations to explore the rich dynamics of the proposed fractal-fractional NMIBC model. We investigate the influence of the fractional order α, the fractal dimension β, and key biological parameters on the system's trajectory. For these simulations, we use the baseline parameters from Table 1 unless stated otherwise.

Sensitivity analysis methodology

To assess the impact of biological parameters on the disease progression, we performed a local sensitivity analysis on the basic reproduction number $\mathcal{R}_0$. We utilized the normalized forward sensitivity index (NFSI), also known as elasticity. This method measures the relative change in $\mathcal{R}_0$ with respect to a relative change in a parameter p, defined as:

$$\Upsilon_p^{\mathcal{R}_0} = \frac{\partial \mathcal{R}_0}{\partial p} \times \frac{p}{\mathcal{R}_0}. \tag{8.1}$$

A positive index implies that an increase in the parameter p increases $\mathcal{R}_0$ (destabilizing the disease-free state), while a negative index indicates a decrease in $\mathcal{R}_0$ (stabilizing the disease-free state). The results of this analysis are visualized in Figure 5b.

9. Results and discussion

The numerical experiments in the previous sections provide a comprehensive view of the fractal-fractional NMIBC model's behavior. This section interprets these findings, connecting the mathematical results to their biological implications for tumor-immune dynamics under chemotherapy.

First, the comparative analysis in Section 7 (Table 4 and Figure 2) serves as a crucial validation of our semi-analytical approach. The results from the 10-term FF-ADM solution are in excellent agreement with the high-order fractional Adams-Bashforth (FAB) method, with negligible error. In contrast, the first-order fractional Euler method (FEM) shows significant divergence, as expected. Furthermore, the convergence analysis (Table 5 and Figure 3) confirms that the numerical schemes

behave precisely as theory predicts: The FEM converges at a rate of $O(h^{\alpha})$ and the FAB method at $O(h^{1+\alpha})$. This gives us high confidence that the FF-ADM is a robust and accurate tool for solving our proposed model.

The core findings of this paper are presented in Figure 4. This figure explores the profound impact of the fractal-fractional operators themselves. Figure 4a shows the effect of varying the fractional order α, which represents memory. As α decreases from 1.0 (the classical model) to 0.85, all system dynamics are slowed. The tumor decays more slowly, but the effector cell population also activates and rises more slowly. This is a critical insight: Strong memory effects in a biological system imply that the system is sluggish and will take longer to reach its steady state. Clinically, this suggests that patient-specific memory effects could be a factor in why some tumors take much longer to clear than others, even with identical parameters. Figure 4b shows the influence of the fractal dimension β. This parameter reflects the geometric complexity of the tumor microenvironment. A lower β (e.g., 0.85) implies a more complex, fractal-like space, which can hinder the diffusion of the MMC drug and the migration of effector cells. The plot shows that, similar to α, a lower β slows down the entire system. This provides a physical mechanism, distinct from temporal memory, for the non-ideal and delayed responses often observed in clinical practice.

Figure 5 extends this analysis. The 2D phase portrait (Figure 5a) reveals a non-obvious consequence of the FF operators. The trajectory of the integer-order model ($\alpha = 1, \beta = 1$) and the FF model ($\alpha = 0.9, \beta = 0.9$) are not the same. They follow different paths from the initial state to the disease-free equilibrium. This implies that the memory and fractal properties do not just scale time; they fundamentally alter the transient interplay between the tumor and the immune system. The sensitivity analysis in Figure 5b provides a guide for therapeutic strategy. The basic reproduction number $\mathcal{R}_0$ is, as expected, most strongly increased by the tumor's own proliferation rate (r). More importantly, it is most strongly decreased by the immune kill rate (p_2), the effector cell production rate (d_0), and the effector cell lifespan (related to μ_2). This quantitatively confirms that strategies aimed at boosting the patient's immune response are the most effective levers for driving $\mathcal{R}_0 < 1$ and achieving tumor clearance in Figures 6 and 7.

Finally, the 3D surface plots visualize the model's key bifurcations. Figure 8a is a clear visualization of the transcritical bifurcation. It shows that as the tumor proliferation rate r increases, the system abruptly shifts from a state of tumor elimination ($T \to 0$) to one of tumor persistence ($T \to T^* > 0$). This is the practical manifestation of $\mathcal{R}_0$ crossing the threshold of 1. Figure 9a provides the therapeutic counter-argument: It shows that by increasing the effector cell production rate d_0 (e.g., via immunotherapy), the system can be forced back across the bifurcation, pushing a persistent tumor into elimination. This provides strong theoretical support for combination chemo-immunotherapy.

The 3D phase-space attractor in Figure 9b provides a holistic view of a treatment failure. In a scenario where $\mathcal{R}_0 > 1$, the system does not spiral toward the DFE (where $T = 0$). Instead, it converges to the stable endemic equilibrium (EE), a state where the drug, a persistent tumor, and an activated (but insufficient) immune response all co-exist. This mathematically describes a chronic, treatment-resistant disease state.

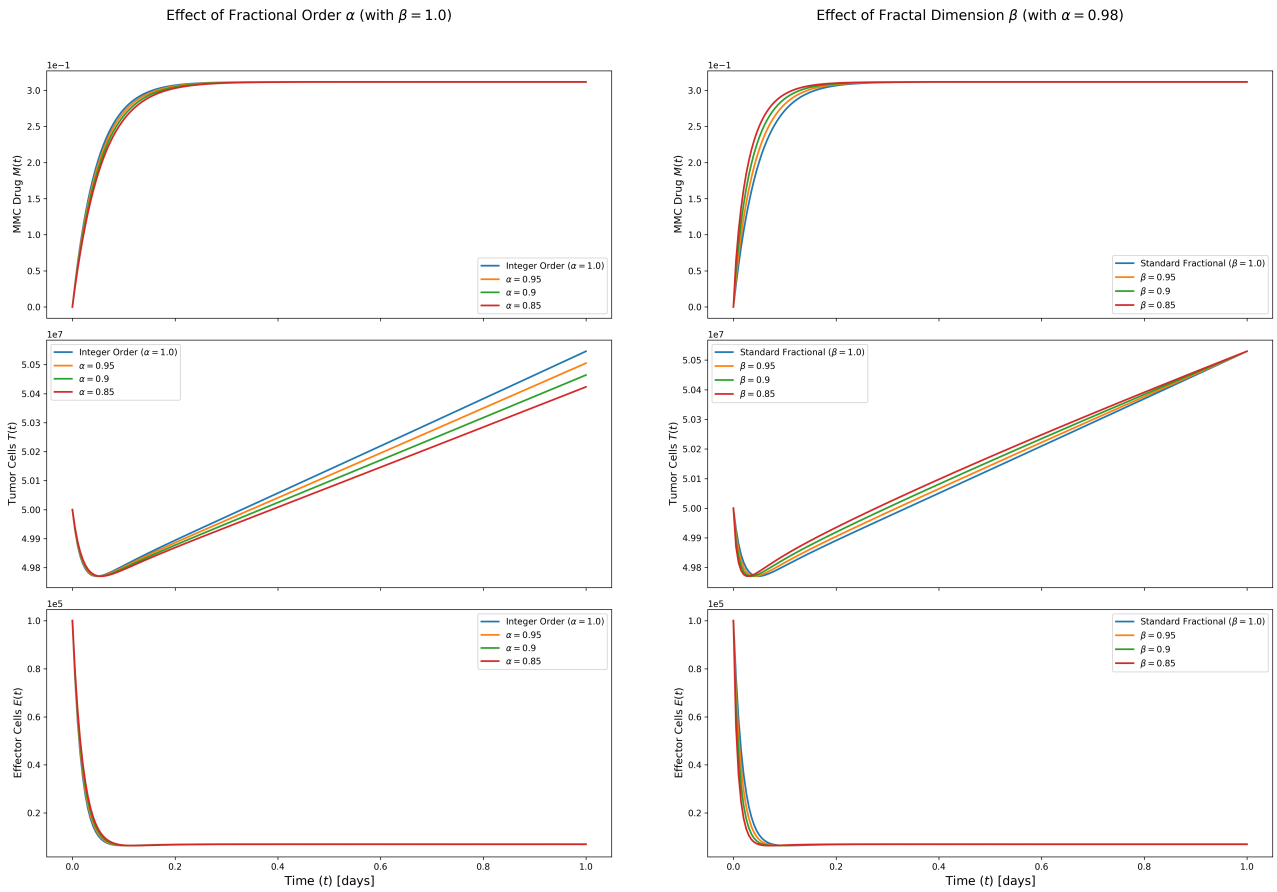

(a) Effect of fractional order α ($\beta = 1.0$)

(b) Effect of fractal dimension β ($\alpha = 0.98$)

Figure 4. Impact of the fractal-fractional operators on the dynamics of $M(t)$, $T(t)$, and $E(t)$. (a) Varying the fractional order α while keeping $\beta = 1$ shows that lower values of α (stronger memory) significantly slow the system's convergence to the steady state. (b) While α governs the intensity of memory (history dependence), β acts as a scaling factor for the time metric (t^{β}). In this 0D system, β phenomenologically captures the macroscopic consequence of spatial heterogeneity: It modifies the effective speed of biological interactions, mimicking the sub-diffusive behavior (anomalous diffusion) characteristic of agents moving through a fractal medium.

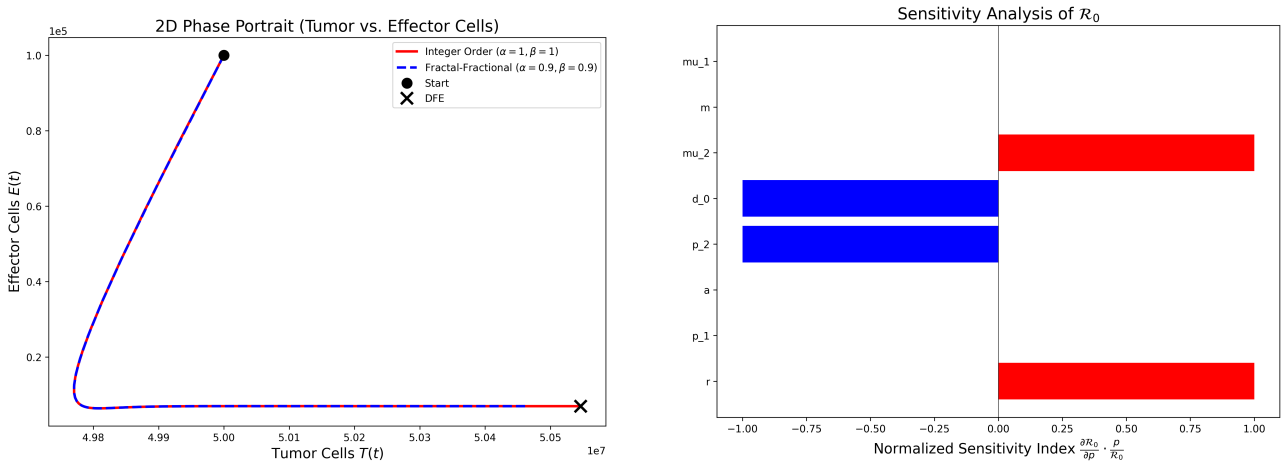

(a) 2D Phase Portrait ($T(t)$ vs. $E(t)$)

(b) Sensitivity Analysis of $\mathcal{R}_0$

Figure 5. (a) A 2D phase-plane analysis comparing the trajectory of the integer-order model ($\alpha = 1, \beta = 1$) with a fractal-fractional case ($\alpha = 0.9, \beta = 0.9$). The paths to the disease-free equilibrium are distinct, highlighting the non-Markovian nature of the FF model. (b) A normalized sensitivity analysis of the basic reproduction number $\mathcal{R}_0$. The tumor proliferation rate (r) has the strongest positive (destabilizing) impact, while immune-related parameters (p_2, d_0, μ_2) have the strongest negative (stabilizing) impact.

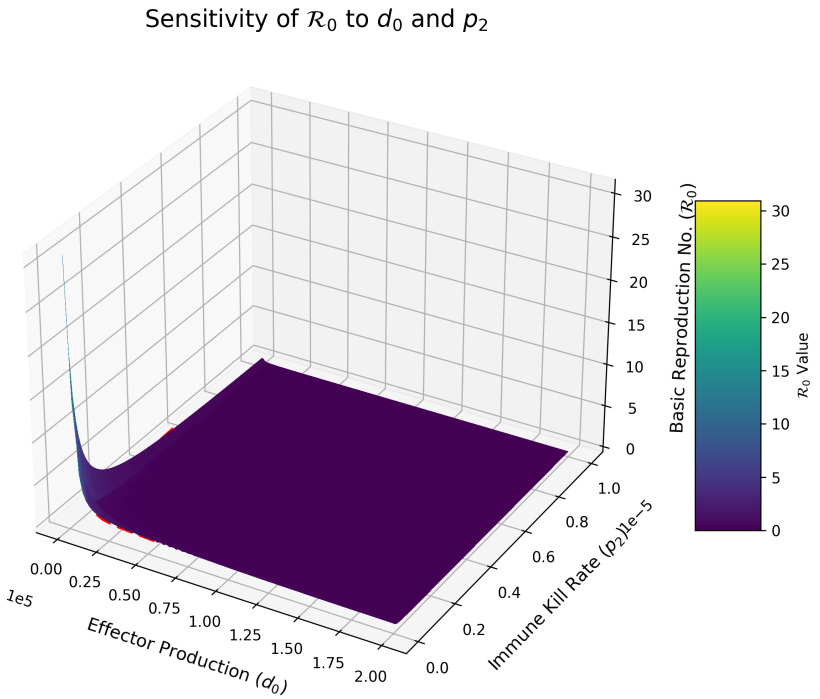

Figure 6. A 3D surface plot illustrating the sensitivity of the basic reproduction number ($\mathcal{R}_0$) to changes in the effector cell production rate (d_0) and the immune cell kill rate (p_2). The red dashed line indicates the critical threshold $\mathcal{R}_0 = 1$, above which the tumor persists.

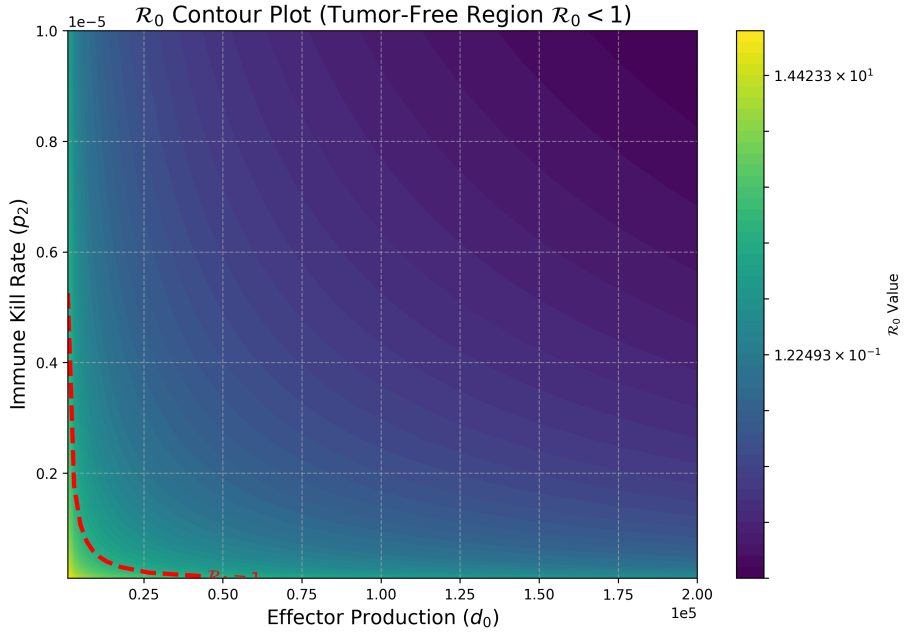

Figure 7. A 2D contour plot showing the relationship between d_0 and p_2 on the value of $\mathcal{R}_0$. The region where $\mathcal{R}_0 < 1$ (the tumor-free state) is stable. The red dashed line represents the $\mathcal{R}_0 = 1$ threshold, which separates tumor elimination from tumor persistence.

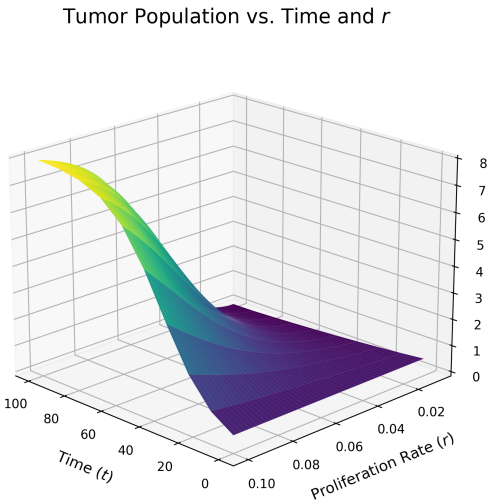

(a) Tumor Population $T(t)$ vs. Time and r

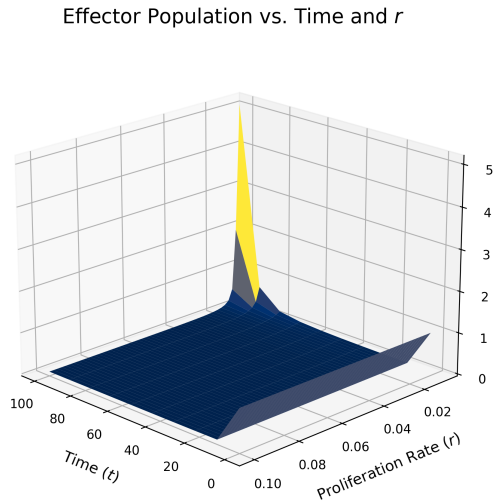

(b) Effector Population $E(t)$ vs. Time and r

Figure 8. 3D surface plots showing the system's dynamics as a function of the tumor proliferation rate r (using $\alpha = 0.98, \beta = 1$). (a) The tumor population $T(t)$ decays for low r, but for r above a certain threshold, it persists and grows, leading to an endemic state. (b) The effector cell population $E(t)$ is shown to be highly responsive to the presence of a growing tumor (higher r), but is ultimately unable to clear it in high-growth scenarios.

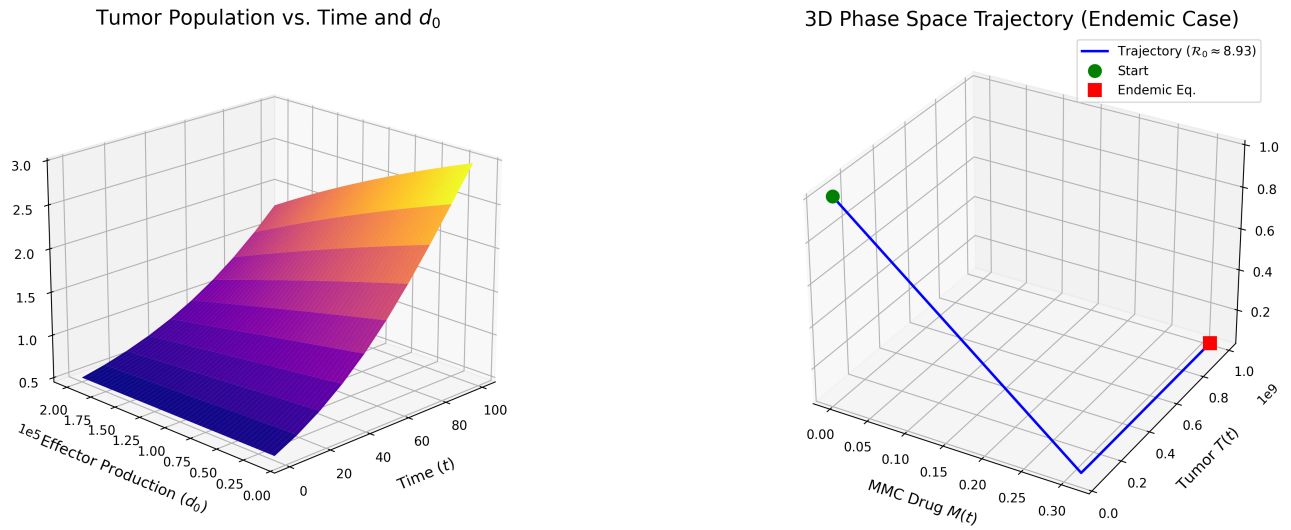

(a) Tumor $T(t)$ vs. Time and d_0

(b) 3D Phase Space Attractor ($\mathcal{R}_0 > 1$)

Figure 9. (a) 3D surface plot of the tumor population $T(t)$ as a function of the effector cell production rate d_0. This clearly shows a critical threshold: below a certain production rate, the tumor persists, while above it, the immune system, aided by MMC, successfully clears the tumor. (b) A 3D phase-space trajectory for an endemic case ($\mathcal{R}_0 > 1.0$), created by simulating a weaker immune response. The solution path converges not to the DFE, but to a stable endemic equilibrium, representing tumor persistence.

10. Conclusion and future scope

10.1. Conclusions

In this paper, we have successfully developed and analyzed a novel fractal-fractional NMIBC model based on the three-compartment integer-order system for MMC chemotherapy. By incorporating the Caputo-type fractal-fractional derivative with order α and dimension β, our model provides a more realistic framework that captures the non-local memory effects of cell interactions and the non-Euclidean, fractal nature of the bladder's tumor microenvironment.

We established the mathematical well-posedness of the model by proving the existence, uniqueness, positivity, and boundedness of its solutions. A rigorous stability analysis was performed, identifying the basic reproduction number ($\mathcal{R}_0$) as the critical threshold. We proved that if $\mathcal{R}_0 \leq 1$, the disease-free equilibrium is globally stable, leading to tumor elimination. If $\mathcal{R}_0 > 1$, a unique endemic equilibrium emerges and becomes globally stable, representing chronic tumor persistence.

A semi-analytical solution was derived using the fractal-fractional Adomian decomposition transform method (FF-ADM), and its accuracy was validated against high-order numerical schemes. Our numerical simulations demonstrated that the fractional parameters α and β are not mere theoretical constructs; they are powerful modulators of the system's dynamics. Lower values of either parameter, representing stronger memory or higher complexity, significantly slow the system's progression, suggesting that these factors could explain patient-specific variations in treatment response time. Sensitivity analysis identified the immune system's parameters (d_0, p_2) as the most potent levers for

controlling the disease, providing a strong rationale for combination chemo-immunotherapy. The 3D bifurcation plots visualize the precise conditions under which treatment succeeds or fails.

10.2. Clinical parameter estimation

Although the present study is primarily theoretical, the fractal-fractional parameters α and β admit meaningful interpretations that enable their estimation from real clinical data. These parameters provide a bridge between the mathematical model and patient-specific biological characteristics.

The fractional order $\alpha \in (0, 1]$ governs the memory effect of the system and, in the present context, reflects delayed immune activation and cumulative treatment response. Clinically, α may be estimated by fitting the model to longitudinal tumor burden data obtained from repeated cystoscopy, histopathology, or imaging-based tumor size measurements. Standard parameter estimation techniques, such as nonlinear least-squares fitting or Bayesian inference applied to time-series data, can be used to identify the value of α that best captures the observed tumor regression or recurrence dynamics, thereby quantifying immune memory effects.

The fractal dimension parameter $\beta \in (0, 1]$ characterizes the geometric complexity of the tumor microenvironment. In practice, β can be inferred from radiomic texture analysis of MRI or CT images, where tumor heterogeneity and irregular vascular structures are known to exhibit fractal-like patterns. Fractal dimension estimates extracted from medical images can be directly incorporated into the model to represent patient-specific tissue complexity and drug diffusion pathways.

Future work will focus on validating the proposed fractal-fractional model through collaboration with clinical oncologists and medical imaging specialists. Such interdisciplinary efforts would enable the integration of patient data for robust parameter estimation, model calibration, and personalized prediction of treatment outcomes in non-muscle-invasive bladder cancer.

10.3. Future scope

The study developed in this study opens several promising avenues for future research:

1. **Clinical Data Validation:** The most critical next step is to fit this fractal-fractional model to real-world clinical data from NMIBC patients. By using longitudinal data on tumor size, recurrence times, and drug concentrations, it may be possible to estimate patient-specific values for α and β, potentially yielding new prognostic biomarkers [57].
2. **Optimal Control Theory:** The current model assumes a constant instillation rate m. A fractal-fractional optimal control problem could be formulated to determine the optimal time-dependent dosing strategy for m that minimizes both the tumor burden and the total drug toxicity.
3. **Stochastic Model:** As demonstrated in recent studies on stochastic dynamics [58], such extensions can capture critical phenomena like extinction probabilities and noise-induced transitions. Therefore, extending our fractal-fractional framework could include stochastic calculus, which remains a primary direction for our future research.
4. **Spatial (PDE) Model:** This work is based on an ODE (0D) model, which assumes all compartments are well-mixed. A future study could extend this to a fractal-fractional partial differential equation (PDE) model to capture the spatial diffusion of MMC into the bladder wall and the heterogeneous distribution of immune and tumor cells.

5. **Expanded Immune Model:** The model could be expanded to include additional cell populations that are critical in NMIBC, such as BCG-activated macrophages, T-regulatory cells (T-regs), and checkpoint molecules (PD-L1), to explore more complex multimodal immunotherapy strategies.

11. Summary of key findings

The primary results and novel insights derived from the analysis of the fractal-fractional NMIBC model are summarized in Table 7.

Table 7. Consolidated summary of key findings and insights.

Title	Figure/Table	Key Insights
Model Equilibrium States	Section 5.1	The model possesses two biologically relevant steady states: The disease-free equilibrium (DFE) and the endemic (tumor) equilibrium (EE).
Stability Threshold	Eq (5.5), Section 5.2	The fate of the tumor is governed by the basic reproduction number $\mathcal{R}_0$. Tumor persistence is guaranteed if $\mathcal{R}_0 > 1$.
Local & Global Stability	Theorems 5.1–5.4	The DFE is locally and globally stable if $\mathcal{R}_0 \leq 1$, while the EE becomes stable for $\mathcal{R}_0 > 1$, indicating a transcritical bifurcation.
Numerical Method Validation	Table 2, Figure 4	The proposed semi-analytical AD-GTM is highly accurate, matching the high-order FAB numerical method.
Numerical Convergence	Table 3, Figure 5	The numerical schemes (FEM, FAB) converge at their respective theoretical rates of $O(h^{\alpha})$ and $O(h^{1+\alpha})$.
Impact of Memory	Figure 4a	A lower fractional order α (stronger memory) significantly slows all system dynamics, increasing the time to tumor clearance.
Impact of Fractal Dimension	Figure 4b	A lower fractal dimension β (higher environmental complexity) also slows the system's progression, mimicking diffusion limitations.
Altered System Trajectory	Figure 7a	The FF operators alter the transient *path* of the chemo-immune interaction, not just its speed, compared to the integer-order model.
Parameter Sensitivity	Figure 7b	$\mathcal{R}_0$ is most sensitive to the tumor growth rate (r) and immune system parameters (p_2, d_0), identifying them as key therapeutic targets.
Tumor Growth Bifurcation	Figure 8a	Increasing the tumor proliferation rate (r) causes a bifurcation from a tumor-free state to a state of stable tumor persistence.
Immunotherapy Efficacy	Figure 9a	Increasing the effector cell production rate (d_0) can reverse the bifurcation, forcing a persistent tumor into elimination.
Endemic State Dynamics	Figure 9b	In a treatment-failure scenario ($\mathcal{R}_0 > 1$), the system converges to a stable endemic attractor where the tumor persists despite treatment.

Author contributions

Sagar R. Khirsariya has written the initial draft of the manuscript with all graphical and tabular results; Saud Fahad Aldosary has analyzed the data and helped in theoretical part. Both authors have reviewed and revised the whole manuscript. All authors approved the final version of the manuscript.

Use of Generative-AI tools declaration

The authors declare they have not used Artificial Intelligence (AI) tools in the creation of this article.

Acknowledgements

The authors would like to express their gratitude to Prince Sattam Bin Abdulaziz University, Saudi Arabia, for providing support for this work under project number (PSAU/2026/R/1447).

Conflicts of interest

The authors have no competing interests to disclose.

References

1. K. Saginala, A. Barsouk, K. Saginala, S. Padala, A. Barsouk, Epidemiology of bladder cancer, *Med. Sci.*, **8** (2020), 15. https://doi.org/10.3390/medsci8010015
2. V. E. Reuter, The pathology of bladder cancer, *Urology*, **67** (2006), 11–17. https://doi.org/10.1016/j.urology.2006.01.037
3. M. Yosef, S. Bunimovich-Mendrazitsky, Mathematical model of MMC chemotherapy for non-invasive bladder cancer treatment, *Front. Oncol.*, **14** (2024), 1352065. https://doi.org/10.3389/fonc.2024.1352065
4. U. Wazir, M. J. Michell, M. Alamoodi, K. Mokbel, Evaluating radar reflector localisation in targeted axillary dissection in patients undergoing neoadjuvant systemic therapy for node-positive early breast cancer: A systematic review and pooled analysis, *Cancers*, **16** (2024), 1345. https://doi.org/10.3390/cancers16071345
5. A. M. Kamat, R. J. Sylvester, A. Böhle, J. Palou, D. L. Lamm, M. Brausi, et al., Definitions, end points, and clinical trial designs for non-muscle-invasive bladder cancer: Recommendations from the international bladder cancer group, *J. Clin. Oncol.*, **34** (2016), 1935–1944. https://doi.org/10.1200/JCO.2015.64.4070
6. A. R. A. Anderson, M. A. J. Chaplain, Continuous and discrete mathematical models of tumour-induced angiogenesis, *B. Math. Biol.*, **60** (1998), 857–899. https://doi.org/10.1006/bulm.1998.0042
7. M. Farman, A. Ahmad, A. Akgül, M. U. Saleem, K. S. Nisar, V. Vijayakumar, Dynamical behavior of tumor-immune system with fractal-fractional operator, *AIMS Math.*, **7** (2022), 8751–8773. http://dx.doi.org/2010.3934/math.2022489

8. T. Lazebnik, Cell-level spatio-temporal model for a bacillus Calmette-Guérin-based immunotherapy treatment protocol of superficial bladder cancer, *Cells*, **11** (2022), 2372. https://doi.org/10.3390/cells11152372

9. S. A. Chrysanthopoulou, T. Hedspeth, D. Antinozzi, A. W. Huang, Y. Sereda, H. Jalal, et al., Simulation models for bladder cancer: A scoping review, *medRxiv*, 2025. https://doi.org/10.1101/2025.03.17.25324125

10. F. Gurcan, S. Kartal, Chaos and its control in a discretized fractional order tumor-immune system model with benign and malignant case, *J. Appl. Math. Comput.*, **71** (2025), 487–515. https://doi.org/10.1007/s12190-025-02491-3

11. K. Dehingia, S. A. Alharbi, A. J. Alqarni, M. Areshi, M. Alsulami, R. D. Alsemiry, et al., Exploring the combined effect of optimally controlled chemo-stem cell therapy on a fractional-order cancer model, *PLoS One*, **20** (2025), e0311822. https://doi.org/10.1371/journal.pone.0311822

12. M. Y. Almusawa, K. Aldawsari, N. Mshary, Exploring fractional dynamics in the fitzhugh-nagumo model with the Caputo operator, *Bound. Value Probl.*, **2025** (2025), 127. https://doi.org/10.1186/s13661-025-02115-6

13. M. Y. Almusawa, K. Aldawsari, N. Mshary, Fractional analysis of nonlinear dynamics in Korteweg-de Vries-Burgers' and modified Korteweg-de Vries equations, *Bound. Value Probl.*, **2025** (2025), 165. https://doi.org/10.1186/s13661-025-02147-y

14. K. A. Rashedi, M. Y. Almusawa, H. Almusawa, T. S. Alshammari, A. Almarashi, Fractional dynamics: Applications of the Caputo operator in solving the Sawada–Kotera and Rosenau–Hyman equations, *Mathematics*, **13** (2025), 193. https://doi.org/10.3390/math13020193

15. A. Alshareef, Quantitative analysis of a fractional order of the SEIcIηVR epidemic model with vaccination strategy, *AIMS Math.*, **9** (2024), 6878–6903. https://doi.org/10.3934/math.2024335

16. K. Ramalakshmi, B. S. Vadivoo, K. S. Nisar, S. Alsaeed, The θ-Hilfer fractional order model for the optimal control of the dynamics of Hepatitis B virus transmission, *Results Control Opti.*, **17** (2024), 100496. https://doi.org/10.1016/j.rico.2024.100496

17. M. Caputo, Linear models of dissipation whose Q is almost frequency independent—II, *Geophys. J. Int.*, **13** (1967), 529–539. https://doi.org/10.1111/j.1365-246X.1967.tb02303.x

18. A. A. Kilbas, H. M. Srivastava, J. J. Trujillo, *Theory and applications of fractional differential equations*, Elsevier, 2006. https://doi.org/10.1016/S0304-0208(06)80001-0

19. L. Sadek, A. Algefary, Efficient scheme for solving tempered fractional quantum differential problem, *Fractal Fract.*, **9** (2025), 709. https://doi.org/10.3390/fractalfract9110709

20. S. Soulaimani, A. Kaddar, Analysis and optimal control of a fractional order seir epidemic model with general incidence and vaccination, *IEEE Access*, **11** (2023), 81995–82002. https://doi.org/10.1109/ACCESS.2023.3300456

21. N. Laksaci, A. Boudaoui, S. M. Al-Mekhlafi, A. Atangana, Mathematical analysis and numerical simulation for fractal-fractional cancer model, *Math. Biosci. Eng.*, **20** (2023), 18083–18103. https://doi.org/10.3934/mbe.2023803

22. S. Swain, S. Swain, B. Panda, M. C. Tripathy, Modeling and optimal analysis of lung cancer cell growth and apoptosis with fractional-order dynamics, *Comput. Biol. Med.*, **188** (2025), 109837. https://doi.org/10.1016/j.compbiomed.2025.109837

23. S. Saber, E. Solouma, Advanced fractional modeling of diabetes: Bifurcation analysis, chaos control, and a comparative study of numerical methods Adams–Bashforth–Moulton and Laplace–Adomian-Padé method, *Indian J. Phys.*, **99** (2025), 5151–5169. https://doi.org/10.1007/s12648-025-03712-y

24. H. Gündoğdu, H. Joshi, Numerical analysis of time-fractional cancer models with different types of net killing rate, *Mathematics*, **13** (2025), 536. https://doi.org/10.3390/math13030536

25. E. Y. Salah, B. Sontakke, A. A. Hamoud, H. Emadifar, A. Kumar, A fractal-fractional order modeling approach to understanding stem cell-chemotherapy combinations for cancer, *Sci. Rep.*, **15** (2025), 3465. https://doi.org/10.1038/s41598-025-87308-w

26. K. S. Nisar, M. Sivashankar, S. Sabarinathan, C. Ravichandran, V. Sivaramakrishnan, Evaluating the stability and efficacy of fractal-fractional models in reproductive cancer apoptosis with ABT-737, *J. Inequal. Appl.*, **2025** (2025), 10. https://doi.org/10.1186/s13660-024-03249-4

27. M. Alhazmi, S. M. Mirgani, S. Saber, Hybrid Euler–Lagrange approach for fractional-order modeling of Glucose–Insulin dynamics, *Axioms*, **14** (2025), 800. https://doi.org/10.3390/axioms14110800

28. I. Malmir, New pure multi-order fractional optimal control problems with constraints: QP and LP methods, *ISA T.*, **153** (2024), 155–190. https://doi.org/10.1016/j.isatra.2024.08.003

29. I. Malmir, An efficient method for a variety of fractional time-delay optimal control problems with fractional performance indices, *Int. J. Dynam. Control*, **11** (2023), 2886–2910. https://doi.org/10.1007/s40435-023-01113-9

30. S. Saber, E. Solouma, M. Alsulami, Modeling computer virus spread using ABC fractional derivatives with Mittag-Leffler kernels: Symmetry, invariance, and memory effects in a four-compartment network model, *Symmetry*, **17** (2025), 1891. https://doi.org/10.3390/sym17111891

31. G. Ali, M. Marwan, U. U. Rahman, M. Hleili, Investigation of fractional-ordered tumor-immune interaction model via fractional-order derivative, *Fractals*, **32** (2024), 2450119. https://doi.org/10.1142/S0218348X24501196

32. T. Q. Tang, Z. Shah, E. Bonyah, R. Jan, M. Shutaywi, N. Alreshidi, Modeling and analysis of breast cancer with adverse reactions of chemotherapy treatment through fractional derivative, *Comput. Math. Method. M.*, **2022** (2022), 5636844. https://doi.org/10.1155/2022/5636844

33. A. Ahmad, M. Farman, P. A. Naik, E. Hincal, F. Iqbal, Z. Huang, Bifurcation and theoretical analysis of a fractional-order Hepatitis B epidemic model incorporating different chronic stages of infection, *J. Appl. Math. Comput.*, **71** (2025), 1543–1564. https://doi.org/10.1007/s12190-024-02301-2

34. M. Alhazmi, S. M. Mirgani, A. Alahmari, S. Saber, Application of LAPM and ABM methods to a fractional SCIR model of pneumonia diseases, *AIMS Math.*, **10** (2025), 25667–25707. https://doi.org/10.3934/math.20251137

35. A. O. Yunus, M. O. Olayiwola, M. O. Abanikanda, Modeling a fractional-order chlamydia dynamic with protected intimacy as a strategic control intervention, *Discov. Public Health*, **22** (2025), 491. https://doi.org/10.1186/s12982-025-00856-4

36. Z. Odibat, A new fractional derivative operator with a generalized exponential kernel, *Nonlinear Dynam.*, **112** (2024), 15219–15230. https://doi.org/10.1007/s11071-024-09798-z

37. K. Shah, B. Abdalla, T. Abdeljawad, M. A. Alqudah, A fractal-fractional order model to study multiple sclerosis: A chronic disease, *Fractals*, **32** (2024), 2440010. https://doi.org/10.1142/S0218348X24400103

38. M. Alhazmi, S. M. Mirgani, A. Aljohani, S. Saber, Numerical simulation of a fractional glucose-insulin model via successive approximation and ABM schemes, *AIMS Math.*, **10** (2025), 22817–22849. https://doi.org/10.3934/math.20251014

39. P. A. Naik, M. Farman, A. Zehra, K. S. Nisar, E. Hincal, Analysis and modelling with fractal-fractional operator for an epidemic model with reference to COVID-19 modelling, *Part. Differ. Equ. Appl. Math.*, **10** (2024), 100663. https://doi.org/10.1016/j.padiff.2024.100663

40. A. Khan, K. Shah, T. Abdeljawad, I. Amacha, Fractal fractional model for tuberculosis: Existence and numerical solutions, *Sci. Rep.*, **14** (2024), 12211. https://doi.org/10.1038/s41598-024-62386-4

41. S. Hariharan, L. Shangerganesh, A. Debbouche, V. Antonov, Dynamic behaviors for fractional epidemiological model featuring vaccination and quarantine compartments, *J. Appl. Math. Comput.*, **71** (2025), 489–509. https://doi.org/10.1007/s12190-024-02249-3

42. L. Sadek, A. S. Bataineh, E. M. Sadek, I. Hashim, A general definition of the fractal derivative: Theory and applications, *AIMS Math.*, **10** (2025), 15390–15409. https://doi.org/10.3934/math.2025690

43. A. Granas, J. Dugundji, *Fixed point theory*, Springer, **14** (2003). https://doi.org/10.1007/978-0-387-21593-8

44. S. Banach, Sur les opérations dans les ensembles abstraits et leur application aux équations intégrales, *Fund. Math.*, **3** (1922), 134–181.

45. D. Matignon, *Stability results for fractional differential equations with applications to control processing*, In: Computational engineering in systems applications, Lille, France, **2** (1996), 963–968.

46. I. Podlubny, *Fractional differential equations*, Academic Press, 1998.

47. Y. Li, Y. Q. Chen, I. Podlubny, Stability of fractional-order nonlinear dynamic systems: Lyapunov direct method and generalized Mittag–Leffler stability, *Comput. Math. Appl.*, **59** (2010), 1810–1821. https://doi.org/10.1016/j.camwa.2009.08.019

48. Z. Wu, Y. Cai, Z. Wang, W. Wang, Global stability of a fractional order SIS epidemic model, *J. Differ. Equ.*, **352** (2023), 221–248. https://doi.org/10.1016/j.jde.2022.12.045

49. G. Adomian, *Solving frontier problems of physics: The decomposition method*, Springer Science & Business Media, **60** (2013).

50. A. M. Wazwaz, A new algorithm for calculating adomian polynomials for nonlinear operators, *Appl. Math. Comput.*, **111** (2000), 33–51. https://doi.org/10.1016/S0096-3003(99)00063-6

51. N. A. Obeidat, M. S. Rawashdeh, M. Q. Al Erjani, A novel Adomian natural decomposition method with convergence analysis of nonlinear time-fractional differential equations, *Int. J. Model. Simul.*, 2024, 1–16. https://doi.org/10.1080/02286203.2024.2369772

52. M. Heydari, A. Atangana, A numerical method for nonlinear fractional reaction-advection-diffusion equation with piecewise fractional derivative, *Math. Sci.*, **17** (2023), 169–181. https://doi.org/10.1007/s40096-021-00451-z

53. A. Atangana, Fractal-fractional differentiation and integration: Connecting fractal calculus and fractional calculus to predict complex system, *Chaos Soliton. Fract.*, **102** (2017), 396–406. https://doi.org/10.1016/j.chaos.2017.04.027

54. H. Delavari, D. Baleanu, J. Sadati, Stability analysis of caputo fractional-order nonlinear systems revisited, *Nonlinear Dynam.*, **67** (2012), 2433–2439. https://doi.org/10.1007/s11071-011-0157-5

55. K. Diethelm, *The analysis of fractional differential equations*, Lecture Notes in Mathematics, Springer Berlin, **2004** (2010). https://doi.org/10.1007/978-3-642-14574-2

56. R. Nuca, M. Parsani, On Taylor's formulas in fractional calculus: Overview and characterization for the caputo derivative, *Fract. Calcul. Appl. Anal.*, **27** (2024), 2799–2821. https://doi.org/10.1007/s13540-024-00311-2

57. M. Alhazmi, S. M. Mirgani, A. Alahmari, S. Saber, Hybrid multi-step fractional numerical schemes for human-wildlife zoonotic disease dynamics, *AIMS Math.*, **10** (2025), 21126–21158. https://doi.org/10.3934/10.3934/math.2025944

58. Y. Hao, Y. Luo, J. Huang, L. Zhang, Z. Teng, Analysis of a stochastic HIV/AIDS model with commercial heterosexual activity and Ornstein–Uhlenbeck process, *Math. Comput. Simul.*, **234** (2025), 50–72. https://doi.org/10.1016/j.matcom.2025.02.020

AIMS Press